PHYSICS OF THE GALACTIC CENTER CLOUD G2, ON ITS WAY TOWARD THE SUPERMASSIVE BLACK HOLE

A. BURKERT[1,2,3], M. SCHARTMANN[1,2], C. ALIG[1,2], S. GILLESSEN[2], R. GENZEL[2], T. K. FRITZ[2], AND F. EISENHAUER[2]
[1] University Observatory Munich, Scheinerstrasse 1, D-81679 Munich, Germany; burkert@usm.lmu.de
[2] Max-Planck-Institute for Extraterrestrial Physics, Giessenbachstrasse 1, 85758 Garching, Germany

ABSTRACT

We investigate the origin, structure, and evolution of the small gas cloud G2, which is on an orbit almost straight into the Galactic central supermassive black hole (SMBH). G2 is a sensitive probe of the hot accretion zone of Sgr A*, requiring gas temperatures and densities that agree well with models of captured shock-heated stellar winds. Its mass is equal to the critical mass below which cold clumps would be destroyed quickly by evaporation. Its mass is also constrained by the fact that at apocenter its sound crossing timescale was equal to its infall timescale. Our numerical simulations show that the observed structure and evolution of G2 can be well reproduced if it forms in pressure equilibrium with its surroundings in 1995 at a distance from the SMBH of 7.6×10^{16} cm. If the cloud had formed at apocenter in the "clockwise" stellar disk as expected from its orbit, it would be torn into a very elongated spaghetti-like filament by 2011, which is not observed. This problem can be solved if G2 is the head of a larger, shell-like structure that formed at apocenter. Our numerical simulations show that this scenario explains not only G2's observed kinematical and geometrical properties but also the Brγ observations of a low surface brightness gas tail that trails the cloud. In 2013, while passing the SMBH, G2 will break up into a string of droplets that within the next 30 years will mix with the surrounding hot gas and trigger cycles of active galactic nucleus activity.

Key words: galaxies: active – galaxies: ISM – Galaxy: center – Galaxy: nucleus

Online-only material: color figures

1. INTRODUCTION

The Galactic center is one of the most extreme and puzzling places in the Milky Way. Harboring a supermassive black hole (SMBH) with a mass of $M_{\rm BH} = 4.31 \times 10^6 \, M_\odot$ (Ghez et al. 2008; Gillessen et al. 2009; Genzel et al. 2010) at the position of the radio source Sgr A*, it is by far the closest and most ideal place to investigate the physics of galactic nuclei and their activity cycles when gas accretes onto the SMBH. Most galaxies contain SMBHs that correlate well with various global galactic properties (Gültekin et al. 2009; Burkert & Tremaine 2010; Kormendy et al. 2011). However, only a small number are observed to be active at any time (e.g., Heckman et al. 2004; King & Pringle 2007). The processes that lead to these long phases of quiescence with no or little SMBH accretion, interrupted by short periods of activity, have not been well understood until now.

The Milky Way's central SMBH is currently classified as inactive, despite observations of irregular flickering events (Baganoff et al. 2001; Genzel et al. 2003) that demonstrate that it is still sporadically accreting small amounts of mass. The "X-ray echo" in the molecular clouds near Sgr A* might be a signature of such an accretion event that occurred a few hundred years ago with an energy output of order $10^{39} \, \mathrm{erg \, s^{-1}}$ (Sunyaev et al. 1993; Koyama et al. 1996, 2003, 2009; Revnivtsev et al. 2006; Goldwurm 2011; Odaka et al. 2011). A major outburst might also have occurred as a by-product of the event that formed the ∼100 massive, young O- and Wolf–Rayet stars that have been found within the central 0.1 pc (Genzel et al. 2003; Ghez et al. 2005; Bartko et al. 2009). Many of these stars orbit Sgr A* in two counter-rotating and inclined disks that probably formed from one or two massive gas clouds that fell into the Galactic nucleus

≲1–10 Myr ago. In addition, numerical simulations show that a $10^5 \, M_\odot$ cloud interacting with the SMBH would naturally form a thin, dense accretion disk that cools and condenses into a disk of massive stars in its self-gravitating parts, outside the SMBH's Bondi radius $R_B \approx 0.1$ pc (Baganoff et al. 2003), in good agreement with the radius regime of the observed stellar disks (e.g., Nayakshin et al. 2007; Bonnell & Rice 2008; Hobbs & Nayakshin 2009; Alig et al. 2011). Alexander et al. (2012), however, point out that a long-lived, gravitationally stable, optically thick residual gas disk should be left behind within R_B, feeding the SMBH on timescales longer than 10 Myr (Nayakshin & Cuadra 2005). Observations completely rule out such a compact disk, which would be easily detectable in the mid-IR (Schödel et al. 2011). The puzzle of the missing gas disk is still poorly understood. It is, however, consistent with the quiescent, low-luminosity active galactic nucleus state of Sgr A* (Loeb 2004) with very low Eddington accretion rates of ≲$10^{-6} \, \dot{M}_{\rm Edd}$ (Baganoff et al. 2001; Bower et al. 2003).

Instead of cold gas, *Chandra* observations of the Galactic center have revealed a tenuous, hot, ionized, X-ray emitting gas bubble (Baganoff et al. 2003) with temperatures of order 1–4 keV that is believed to originate from the shock-heated strong stellar winds of surrounding massive stars (Melia 1992; Krabbe et al. 1991; Najarro et al. 1997). Chevalier (1992) investigated the outflow of this hot gas from the central 0.8 pc of the Galaxy and the formation of a shocked wind bubble. Rockefeller et al. (2004) showed that such a wind could explain the diffuse X-ray emission of the inner 1–2 pc region. Wind material, however, should also be gravitationally captured and should accrete onto Sgr A* (e.g., Melia et al. 1992; Wardle & Yusef-Zadeh 1992; Melia 1992; Ruffert & Melia 1994). Estimates of the Bondi–Hoyle mass accretion onto Sgr A* lead to rates of $\dot{M} \approx 10^{-6}$–$10^{-5} \, M_\odot \, \mathrm{yr^{-1}}$ (Coker & Melia 1997; Cuadra et al. 2006, 2008, Quataert 2002, 2004), which would

---
[3] Max-Planck Fellow.

imply accretion luminosities of $L \approx 0.1\dot{M}c^2 \geqslant 10^{40}\,\mathrm{erg\,s^{-1}}$ that are much higher than the observed bolometric luminosity of order $10^{35}\,\mathrm{erg\,s^{-1}}$ (Baganoff et al. 2003; Yusef-Zadeh & Wardle 2010) or the accretion rates of $\leqslant 2 \times 10^{-7}\,M_{\odot}\,\mathrm{yr^{-1}}$, as inferred from Faraday rotation measurements (Marrone et al. 2007). An important parameter that affects the accretion luminosity is the radiative efficiency of the accretion material. Various radiatively inefficient accretion flow models have been constructed (e.g., Narayan & Yi 1994; Quataert & Narayan 1999; Narayan 2002; Yuan et al. 2003); these store most of the viscously dissipated energy in the gas that is being advected into the SMBH with only a small fraction of this energy being lost by radiation. Most of the energy liberated in the shocked stellar winds or subsequently in the accretion flow and most of the hot gas could also be lost either as an outflowing central star cluster wind or as magnetically driven wind (e.g., Coker & Melia 1997; Stone et al. 1999; Hawley & Balbus 2002; Quataert 2002, 2004; Narayan et al. 2003; Cuadra et al. 2005, 2006; Tanaka & Menou 2006). Mass loss could significantly reduce the gas density close to the SMBH. Sazonov et al. (2012) point out that such a reduction in hot gas density inside the Bondi radius could still be in agreement with *Chandra* observations if a substantial or even dominant fraction of the X-ray emission is actually produced by late-type main-sequence stars of the central stellar cusp.

The situation is even more complex. The detailed three-dimensional numerical simulations of the stellar wind inter-action of the young massive stars in the Galactic center (Cuadra et al. 2005, 2006, 2008; Nayakshin et al. 2007; Nayakshin & Cuadra 2007; Martins et al. 2007) demonstrate that fast winds from Wolf–Rayet stars with velocities of $v_w \geqslant 1000\,\mathrm{km\,s^{-1}}$ are shock heated to temperatures $>10^7$ K. In contrast, luminous blue variable stars with wind velocities of 300–600 km s^{-1}, when shocked, generate gas with temperatures of 10^6 K that can cool quickly and form cold, ionized 10^4 K gas clumps and filaments that fall onto the SMBH, leading to short bursts of activity. In this case, the accretion rate of the SMBH, averaged over times of the order of a typical clump infall timescale, could be much larger than estimated from its current interburst X-ray luminos-ity. The existence of such a cold gas component would therefore have strong implications for our understanding of the activity and growth of the Milky Way's SMBH.

Strong observational evidence for a cold cloud component in the Galactic center has recently been reported by Gillessen et al. (2012). They detected a dense, dusty, and ionized gas clump, which we will call G2 (another cloud, G1, had been discovered earlier by Clênet et al. 2005), with a dust temperature of merely 550 K and a gas temperature of order 10^4 K, representing a relatively cold droplet of ionized gas, embedded in the diffuse 10^8 K gas of the central hot bubble. The cloud's radius is resolved in the direction of its orbital motion but unresolved in the perpendicular direction. Gillessen et al. (2012) adopted an effective, spherical radius in 2011.3 of 15 mas that corresponds to 1.875×10^{15} cm. For case B recombination and a mean molecular weight of $\mu = 0.6139$, the observed Brγ luminosity implies a cloud density of $\rho_c \approx 6.1 \times 10^{-19} f_V^{-1/2}\,\mathrm{g\,cm^{-3}}$ with a corresponding cloud mass of $M_c \approx 1.7 \times 10^{28} f_V^{1/2}$ g, or approximately 3 Earth masses. Here $f_V \leqslant 1$ is the volume filling factor. In this paper, we will investigate scenarios in which the cloud is a compact region of cold gas; we therefore adopt $f_V = 1$. The observations (contours in Figure 5; see also Figure 2 in Gillessen et al. 2012) also indicate that G2 might be the upstream compact head of a larger, diffuse distribution of cold gas. The total mass of this system could be substantially larger than G2's estimated mass.

The cloud is approaching Sgr A*. Its orbit could be traced back for the past 10 years, allowing a detailed orbital analysis that shows that G2 is moving on a highly eccentric orbit. In 2013.5 the cloud will pass the SMBH at a pericenter distance of merely 3100 times the event horizon, corresponding to $4.0 \pm 0.3 \times 10^{15}$ cm. The next two years will therefore provide a unique opportunity to investigate directly the disruption of a cold gas clump by its gravitational interaction with the SMBH and perhaps even the onset of a new activity cycle, triggered by the accretion of gas onto the central black hole. In fact, clear evidence for ongoing tidal velocity shearing and stretching has already been detected.

The existence of a tiny, cold gas cloud in the near vicinity of the SMBH, embedded in the hostile $\sim 10^8$ K gaseous environ-ment, is surprising and raises numerous interesting questions: From where did this cloud come, and where will it go? Why is it on such a highly eccentric orbit? Which processes constrain the physical properties of G2, i.e., its size, mass, density, tem-perature and geometrical shape. How many clouds like G2 are currently orbiting Sgr A*, and how do they affect its activity and gas accretion rate?

In this paper we will investigate some of these questions, focusing on a simplified prescription of the cloud's structure and evolution. More detailed numerical simulations will be presented in subsequent papers. Section 2 discusses possible formation scenarios. Section 3 summarizes the orbital properties of G2 which have implications for its formation. Section 4 investigates the various hydrodynamical processes of interaction between G2 and its surrounding that constrain G2's origin, orbit and evolution. In Section 5 we show that G2 can in turn be used as a sensitive probe to explore the thermodynamics of the diffuse gas component in the Galactic center. Finally, Section 6 presents a first set of hydrodynamical simulations that explore the evolution of a cold gas cloud, moving through a hot, stratified medium within the gravitational potential of the SMBH. The results are summarized and conclusions are drawn in Section 7.

2. FORMATION SCENARIOS

Possible formation scenarios can be broadly subdivided into two categories: the cloud scenario versus the compact source scenario.

2.1. The Cloud Scenario

The cloud model assumes that G2 is a cold gas clump, embedded in and confined by the hot gaseous environment of the central bubble. For the densities and temperatures of the diffuse hot gas in the Galactic center, the cooling timescale of the hot gas is much longer than the dynamic timescale (Cuadra et al. 2005; Quataert 2004). Cloud formation due to a cooling instability (Field et al. 1969; Burkert & Lin 2000) of the hot gas can therefore be ruled out as a formation mechanism. The most likely scenario is that G2 originates from the complex two-phase medium in one of the two disks of young massive stars that surround the central bubble. Shocked, fast winds of young massive stars with velocities of order 1000 km s^{-1} generate hot 10^7 K plasma, which partly is gravitationally captured by the SMBH, forming the central hot bubble. In contrast, slow winds from luminous blue variable candidates with velocities of 300–500 km s^{-1} when shocked are heated only to 10^6 K and subsequently cool quickly, leading to the formation of cold,
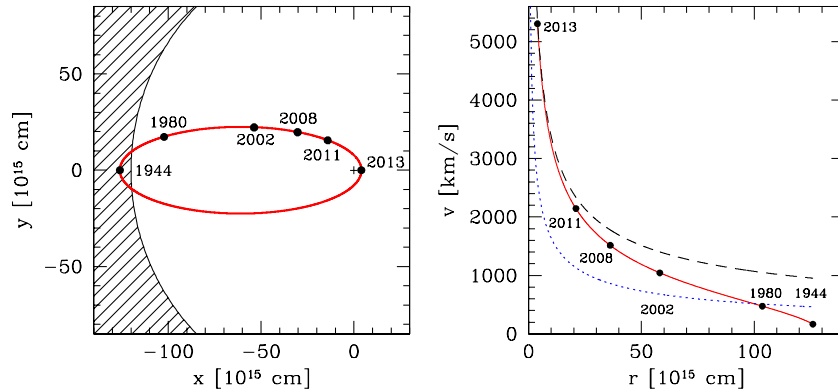
Figure 1. Left panel shows the orbit and location of G2 in the orbital plane. G2's apocenter coincides with the inner edge of the clockwise rotating stellar disk (shaded area). The cloud will pass the SMBH (cross) in 2013 at a distance of merely ∼3100 times the event horizon. Due to its highly eccentric orbit, the cloud spends most of its time in the outer regions. The right panel shows the velocity of G2 as function of its distance r from the SMBH. For comparison, the dashed line shows a parabolic, unbound orbit with total energy $E = 0$. The dotted line shows the local sound speed of the diffuse, hot environment (Equation [3]).

(A color version of this figure is available in the online journal.)

bound cloudlets embedded in the hot intercloud medium (Koo & McKee 1992). Interestingly, the orbital plane of G2 coincides with the clockwise disk of young, massive O and Wolf–Rayet stars, and its apocenter distance agrees with the disk's inner edge (the left panel of Figure 1). This supports the notion that the cloud might indeed be shocked wind debris. The circular velocities of the stars in the disk are of order $700 \, \mathrm{km \, s^{-1}}$, while G2 started on a highly eccentric orbit with a tangential velocity at apocenter of order $200 \, \mathrm{km \, s^{-1}}$ (see Section 3). For typical wind velocities of order $500 \, \mathrm{km \, s^{-1}}$ and assuming a rotational velocity of the star of order $700 \, \mathrm{km \, s^{-1}}$, clumps might then have rotational velocities that range between $1200 \, \mathrm{km \, s^{-1}}$ upstream and $200 \, \mathrm{km \, s^{-1}}$ downstream. While the upstream clumps might be ejected from the Galactic center, downstream clumps would have just the correct initial velocity to fall into the center on a highly eccentric orbit, like G2. One of the implications of this model is that cold clumps with a large spectrum of masses and orbital parameters should continuously be produced by this process in the stellar disks, with many of them falling into the central region on a highly eccentric orbit. We will show, however, in the subsequent sections that G2's mass is special in the sense that clumps with masses larger than that of G2 might easily break up into smaller pieces, while smaller clumps evaporate quickly.

2.2. The Compact Source Scenario

Within the framework of the compact source scenario, G2 represents the visible diffuse gas atmosphere of an unresolved dense object in its center that might continuously lose gas (Gillessen et al. 2012; Murray-Clay & Loeb 2012). The object might have formed 10^6 yr ago in the stellar disk and was scattered into a highly eccentric orbit due to a close encounter with another star or massive black hole. Gillessen et al. (2012) argue that the gas cloud must be optically thin. In order to be invisible, its central compact object has to be either hotter than $10^{4.6}$ K, emitting most of its light in the ultraviolet with a low enough luminosity of $<10^{3.7} \, L_\odot$, or very cold. Gillessen et al. suggest a compact planetary nebula as a possible candidate. Murray-Clay & Loeb (2012) propose a dense, protostellar disk bound to a low-mass star. Another possibility might be an evaporating low-mass star, brown dwarf, or Jupiter-like planet.

In order to distinguish between the different scenarios and determine G2's nature, it is important to find constraints that

must be met by any viable model. In the following sections, we will investigate characteristic properties of G2's structure and orbit, which provide information about its origin. We will then focus on the cloud scenario in detail using hydrodynamical simulations that follow the cloud on its way toward pericenter and dispersal afterward.

3. ORBITAL PARAMETERS OF G2 AND ITS BIRTH LOCATION

Measurements of the position and velocity of G2 tightly constrain its orbit (see Gillessen et al. 2012 for details). Adopting an SMBH mass of $4.31 \times 10^6 \, M_\odot$ and a Sun–Galactic-center distance of 8.33 kpc, the orbital eccentricity is $e = 0.9384 \pm 0.0066$, with a period of 137.8 ± 11 years and a semimajor axis of $6.49 \pm 0.35 \times 10^{16}$ cm. The left panel of Figure 1 shows the orbit of the cloud. For a Keplerian orbit, G2 would have been at apocenter in the year 1944.6, with a distance from the SMBH of $r_{\mathrm{apo}} = 1.26 \pm 0.06 \times 10^{17}$ cm. In 2011.5 its distance was 1.8×10^{16} cm. It will reach pericenter in 2013.5, with a distance of merely $r_{\mathrm{peri}} = 4.0 \pm 0.3 \times 10^{15}$ cm. Due to its highly eccentric orbit, the cloud spends most of its time at large radii $r \geqslant 5 \times 10^{16}$ cm.

Our simulations (Section 6) show that the cloud will not survive its pericenter passage. If it formed close to its presently observed radius ("in situ" scenario; see Section 6.1), we would be very fortunate to have discovered it before its disruption. Although such a coincidence cannot be ruled out, it is more likely that the cloud formed close to apocenter at $r \geqslant 10^{17}$ cm at the inner edge of the clockwise disk (shaded area in the left panel of Figure 1).

The right panel of Figure 1 shows the velocity of the cloud as a function of its distance from the SMBH. If G2 started at apocenter, its velocity would be $v = 168 \pm 80 \, \mathrm{km \, s^{-1}}$ which is much smaller than its circular velocity of $676 \, \mathrm{km \, s^{-1}}$. In 2011.5 its velocity had increased to $v = 2360 \pm 50 \, \mathrm{km \, s^{-1}}$ and at pericenter it will have accelerated to a velocity of $5264 \pm 300 \, \mathrm{km \, s^{-1}}$. For comparison, the dashed line corresponds to the velocity expected for an object on a parabolic orbit. The cloud is gravitationally bound to the SMBH with a binding energy per mass of

$$E_b/M_c = \frac{1}{2}v^2 - \frac{GM_{\mathrm{BH}}}{r} = -4.4 \times 10^{15} \, \mathrm{erg \, g^{-1}}. \quad (1)$$

3

For a total cloud mass of $M_c = 1.7 \times 10^{28} f_V^{1/2}$ g, the total binding energy would then be $E_b = -7.5 \times 10^{43} f_V^{1/2}$ erg.

4. INTERACTION WITH THE HOT SURROUNDING GAS

Up until now, we assumed a Keplerian orbit. However, G2's motion is affected by its hydrodynamical interactions with its confining, hot gaseous surroundings (Gillessen et al. 2012). Here, we adopt the Yuan et al. (2003) model (see also Xu et al. 2006), which reproduces the *Chandra* X-ray observations and is consistent with the low accretion rate inferred by Marrone et al. (2007). For a mean molecular weight $\mu = 0.614$ the hot gas density distribution in the surrounding of Sgr A* is

$$\rho_{\text{hot}}(r) = \rho_0 \frac{r_0}{r} = \eta_{\text{hot}} \times 1.7 \times 10^{-21} \left(\frac{10^{16} \text{ cm}}{r} \right) \text{ g cm}^{-3}, \quad (2)$$

where $r_0 = 10^{16}$ cm and $\rho_0 = \rho(r_0)$. $\eta_{\text{hot}} \leqslant 1$ takes into account the fact that some fraction of the observed X-ray luminosity might be due to unresolved stellar sources (Sazonov et al. 2012). Given the density distribution, the assumption that the hot gas component is close to hydrostatic equilibrium within the SMBH's gravitational potential would lead to a temperature distribution

$$T_{\text{hot}}(r) = T_0 \frac{r_0}{r} = \mu \frac{G M_{\text{BH}}}{2 R_g r_0} \frac{r_0}{r} = 2.1 \times 10^8 \left(\frac{10^{16} \text{ cm}}{r} \right) \text{ K} \quad (3)$$

with $T_0 = T(r_0)$. Note that T_0 is independent of the mass loading, i.e., ρ_0. Our estimate of T_0 is a factor of 1.7 smaller than the value adopted by Gillessen et al. (2012), taken from the Xu et al. (2006) model with a temperature of $T_0 = 3.5 \times 10^8$ K. It is, however, more consistent with Yuan et al. (2003, their Figure 2). If the hot gas actually fell inward as expected for an accretion flow, then T_0 would be even lower. If the temperature is as high as that adopted by Xu et al. (2006), the pressure force exceeds the gravitational force, resulting in an expansion that contradicts the gas infall scenario. The blue dotted line in the right panel of Figure 1 shows the sound speed of the hot bubble, adopting Equation (3). The cloud's velocity is sonic with respect to the hot gas in the outer regions and becomes slightly supersonic (Mach 1.5) farther in. We have assumed hydrostatic pressure equilibrium with the gravitational potential of the SMBH. The situation is certainly much more complex. Rotation, convection, thermal winds, heating and cooling processes, thermal conduction and magnetic fields are likely to affect the detailed structure of the hot bubble surrounding Sgr A* (e.g., Stone et al. 1999; Hawley & Balbus 2002; Johnson & Quataert 2007). Given the limited amount of data, it is currently difficult to constrain models that include these effects. In order to keep the theory simple and well determined, we therefore restrict ourselves in this paper to the simple atmosphere, as given by Equations (2) and (3). Our results and predictions might serve as a first approximation and a test for subsequent more sophisticated models.

A detailed investigation of the cloud's evolution and hydrodynamical interaction with its surroundings requires an estimate of its radius R_c and density ρ_c. In this paper, we will follow Gillessen et al. (2012) and assume that the cloud is ionized by the strong UV field of the central cluster of massive stars. Its cooling timescale is (Sutherland & Dopita 1993; Burkert & Lin 2000) $\tau_{\text{cool}} = 3 k_B T_c / \Lambda n_c$, which for a cooling rate of $\Lambda \approx 3 \times 10^{-22}$ erg cm^3 s^{-1}, cloud densities of $n_c \geqslant 10^5$ cm^{-3}

and cloud temperatures of $T_c \approx 10^4$ K leads to $\tau_{\text{cool}} \leqslant 10^5$ sec, which is much shorter than the orbital period. G2 should therefore maintain its temperature of $T_c = 10^4$ K, set by photo ionization equilibrium during most of its evolution. Because of its small mass density with respect to its Roche density, self-gravity is completely negligible. In this case, it will try to achieve a homogeneous density state in pressure equilibrium with the surroundings. The hydrodynamical simulations presented in Section 6 actually show a more complex structure due to the compression of the front edge by ram pressure, while at the same time the back downstream tail is at slightly lower densities due to tidal shearing. This, however, does not affect much the cloud's effective size, which for most of its orbit is well reproduced by adopting a mean density that is consistent with the assumption of pressure equilibrium: $\rho_c = \rho_{\text{hot}} T_{\text{hot}} / T_c$.

Unfortunately, the observations do not resolve G2's minor axis, perpendicular to the orbital motion. They only provide an upper limit of 12 mas, corresponding to $R_c \leqslant 1.5 \times 10^{15}$ cm. The 2008.3 position versus line-of-sight velocity (PV) diagram (the left panel of Figure 5), however, shows a velocity gradient that can be used to determine the elongation of the cloud along its orbit, which in this stage corresponds to a major axis radius of 21 mas or 2.6×10^{15} cm. Adopting a cylindrical shape as expected for a tidally elongated object, a lower limit of its density in 2008 was then $\rho_c \geqslant 5 \times 10^{-19}$ g cm^{-3}. The cloud has been in this compact state from the earliest spectral measurements, dating back to 2002 until 2008. In 2011.5 (the middle panel of Figure 5), the cloud developed a much stronger velocity shear due to the gravitational acceleration. Its corresponding major-axis length was 22 mas or 2.75×10^{15} cm, leading to a cloud density that did not change much until 2008 if one adopts a constant minor axis radius. As the minor-axis is not resolved, the cloud's density in 2011 could, however, be substantially larger than in 2008, as it might have been stretched and compressed into a dense, thin, spaghetti-like filament (see Section 6).

Several nonlinear and complex hydrodynamical processes dominate G2's interaction with its surrounding, diffuse gas. These include evaporation, ram pressure, gas stripping, cloud compression, or expansion as well as Rayleigh–Taylor and Kelvin–Helmholtz instabilities. In addition, the cloud might be affected by compressional heating and cooling and might be threaded by magnetic fields. A detailed investigation of all these simultaneously acting processes requires self-consistent numerical simulations that are beyond the scope of this paper. Here we restrict ourselves to some of the more basic aspects, leaving more detailed models to subsequent papers. We start with a discussion of the more dominant processes in isolation and then present a first set of numerical simulations that investigate especially the tidal effects on G2's evolution.

4.1. Cloud Ablation

As G2 moves through the surrounding gas, material will be ablated from the cloud. This process has been studied in detail in a different context by Kwak et al. (2011; see also Vieser & Hensler 2007a, 2007b; Heitsch & Putman 2009), who investigated the evolution of a high-velocity cloud traveling through hot gas in the Galactic halo. Kwak et al. (2011) found an ablation mass-loss rate that is proportional to the geometrical cross section of the cloud. This can be understood if the mass-loss rate is proportional to the flux of diffuse gas encountering the cloud

$$\frac{dM_c}{dt} = -q_{\text{abl}} \pi R_c^2 \rho_{\text{hot}} v \quad (4)$$

with v being the velocity of the cloud through the hot medium. An investigation of the numerical simulations of Kwak et al. (2011; see their Figure 3) shows that the ablation efficiency $q_{abl} \approx 0.004$. For a constant cloud density ρ_c, the cloud's radius changes as

$$\frac{d R_c}{dt} = -0.25 q_{abl} v \frac{\rho_{hot}}{\rho_c} \qquad (5)$$

which leads to an ablation timescale of

$$\tau_{abl} = \frac{R_c}{0.25 q_{abl} v} \frac{\rho_c}{\rho_{hot}} = 6 \times 10^6 \,\text{yr} \left(\frac{R_c}{2 \times 10^{15}\,\text{cm}} \right)$$
$$\times \left(\frac{10^3\,\text{km s}^{-1}}{v} \right) \left(\frac{\rho_c/\rho_{hot}}{10^4} \right) \left(\frac{0.004}{q_{abl}} \right). \qquad (6)$$

At all positions along G2's orbit the ablation timescale is orders of magnitude larger than the orbital timescale. Mass loss by ablation is therefore negligible, even if the ablation efficiency is close to its maximum value of $q_{abl} = 1$.

4.2. Cloud Evaporation

Small gas clouds, embedded in a hot environment, will also lose gas due to evaporation as a result of thermal conduction. The classical thermal conductivity (Spitzer 1962; Parker 1963) is based on the diffusion approximation, which assumes that the electron mean free path λ_e of the hot medium is small compared to the cloud radius R_c. Cowie & McKee (1977) in their seminal paper demonstrate that this approximation is invalid as soon as $\lambda_e \gtrsim R_c$, that is, if the saturation parameter $\sigma_0 = 1.84 \, \lambda_e/R_c > 1$. In this case, the heat flux is no longer determined by the classical diffusion formula.

For the central hot bubble we find

$$\lambda_e = 6 \times 10^3 \left(\frac{T}{K} \right)^2 \left(\frac{10^{-21}\,\text{g cm}^{-3}}{\rho_{hot}} \right) \text{cm}$$
$$= 3 \times 10^{17} \left(\frac{10^{16}\,\text{cm}}{r} \right) \text{cm} \qquad (7)$$

which for all relevant distances r from the SMBH is indeed much larger than G2's observed size R_c. Adopting a typical cloud radius of order $(1-2) \times 10^{15}$ cm, the corresponding saturation parameter is $\sigma_0 \approx 50$–200. In the saturated limit and assuming pressure equilibrium between the cloud and the hot surrounding, the evaporation timescale is given by (Cowie & McKee 1977)

$$\tau_{evap} \approx 64\,\text{yr} \left(\frac{r}{10^{16}\,\text{cm}} \right)^{1/6} \left(\frac{M_c}{1.7 \times 10^{28}\,\text{g}} \right)^{1/3}. \qquad (8)$$

Cowie & McKee (1977) argue that for a wide variety of conditions, the presence of a magnetic field does not strongly affect this timescale. Interestingly, this evaporation timescale is very similar to the infall timescale of 69 yr. Equation (8) provides a strong lower limit on the mass of cold dust clouds that can penetrate as deeply into the hot bubble as observed for G2. Only clouds with masses of the order of or larger than G2 would reach distances of $(1-2) \times 10^{16}$ cm. We also can conclude that, once G2 breaks up at pericenter, its subfragments might dissolve quickly. Note, however, that the mixing of cloud material with the diffuse surrounding will change the thermodynamic properties of the bubble. According to Equation (2) the total mass of hot gas in the inner 2×10^{16} cm is similar to G2's mass. Mixing of cloud debris with the environment could effectively cool the innermost

region of the hot bubble, which would reduce the efficiency of evaporation. In addition, this process might destabilize the atmosphere, which then collapses onto the SMBH. The situation is different in the outer orbital parts, where the mass of the hot bubble is more than a factor of 100 larger than G2's mass.

4.3. Ram Pressure Effects

Ram pressure will compress the cloud into a lenticular and sickle-shaped structure (e.g., Murray & Lin 2004; Schartmann et al. 2011). The importance of ram pressure, compared to the thermal pressure of the surroundings, is given by the ratio v^2/c_{hot}^2, where c_{hot} is the sound speed of the hot gas component. As shown by the blue dashed line in the right panel of Figure 1, close to apocenter, gas pressure dominates, while at its present location ram pressure is a factor of 2–3 larger than the thermal pressure.

The drag will also remove part of the cloud's orbital energy. Given the highly eccentric orbit, we can to a good approximation neglect the cloud's small tangential motion. In this case, the energy lost by G2 on its way from radius r_1 to radius r_2 is (Murray & Lin 2004)

$$\Delta E_{drag} = \frac{1}{2} \pi C_D \int_{r_1}^{r_2} R_c^2 \rho_{hot}(r) v^2(r) dr, \qquad (9)$$

where $C_D \approx 1$ is the drag coefficient. The observations already demonstrate that, within the observational errors, G2 follows a Keplerian orbit. ΔE_{ram} therefore should be small, compared to the cloud's kinetic and absolute potential energy. In this case we can use $v(r)$ from Equation (1) and assume E_b/M_c to be roughly constant. Let us first assume that the cloud does not have enough time to react to the increasing external pressure on its way toward pericenter. In this case, its radius R_c is constant and the integration of Equation (9) leads to

$$\Delta E_{ram}(r) = \pi \rho_0 r_0 C_D R_c^2 \left[\frac{E_b}{M_c} \ln \left(\frac{r_2}{r_1} \right) - G M_{BH} \left(\frac{1}{r_2} - \frac{1}{r_1} \right) \right]. \qquad (10)$$

Adopting $C_D = 1$ and an effective cloud radius of $R_c = 2 \times 10^{15}$ cm, the energy lost between apocenter and $r_{2011.5} = 1.8 \times 10^{16}$ cm due to ram pressure effects would be $\Delta E_{ram}(r_{2011.5}) = 7\eta_{hot} \times 10^{42}\,\text{erg} = 0.09\eta_{hot}E_b$. This confirms that the cloud moves on a ballistic orbit as it approaches the SMBH. It also indicates that our estimate of G2's apocenter is robust. For such an extended cloud, ram pressure effects would, however, change the cloud's orbit substantially within the next 2 years on its way toward pericenter, with $\Delta E_{ram}(r_{peri}) = 5\eta_{hot} \times 10^{43}\,\text{erg} = 0.7\,\eta_{hot}E_b$. It is unlikely that we can assume a fixed size, as the cloud will continuously try to achieve pressure equilibrium with its surroundings. If $\rho_c = \rho_{hot} T_{hot}/T_c$, and adopting a spherical geometry, the energy loss is

$$\Delta E_{ram}(r) = \pi C_D \left(\frac{\rho_0}{r_0} \right)^{1/3} \left(\frac{3 M_c T_c}{4 \pi T_0} \right)^{2/3}$$
$$\times \left[\frac{3}{4} \frac{E_b}{M_c} \left(r_2^{4/3} - r_1^{4/3} \right) + 3 G M_{BH} \left(r_2^{1/3} - r_1^{1/3} \right) \right]. \qquad (11)$$

Now, for $T_c = 10^4$ K, on its way from apocenter to $r_{2011.5}$, the cloud would lose $\Delta E_{ram}(2011.5) = 0.02\eta_{hot}^{1/3}E_b$. This value increases to $0.06\,\eta_{hot}^{1/3}E_b$ until pericenter, which is much smaller
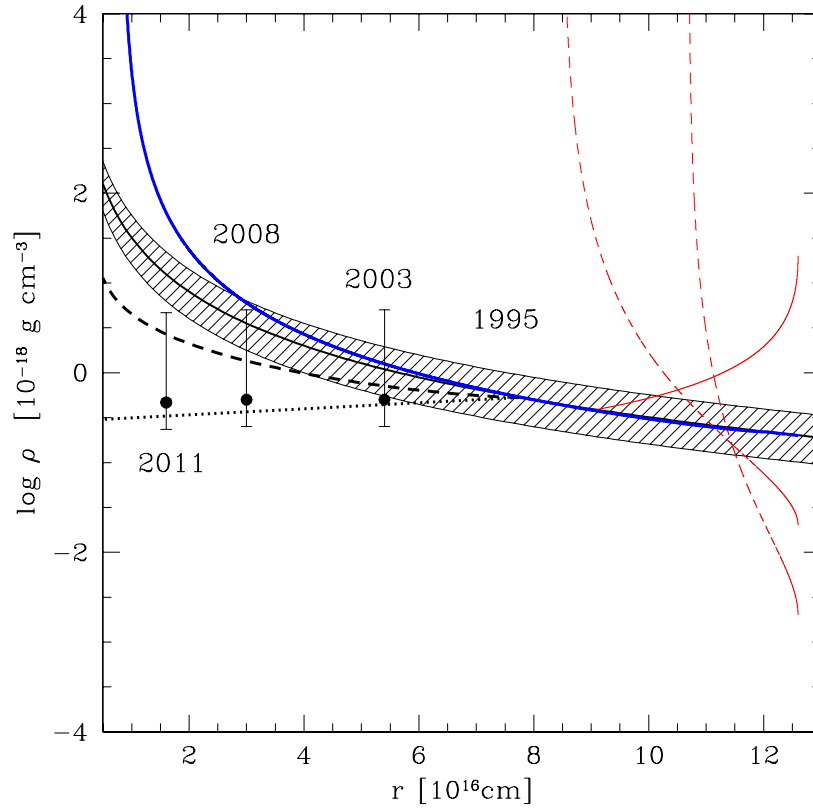
Figure 2. Dashed region shows the expected density of G2 as a function of orbital radius r, assuming pressure equilibrium with the surrounding hot bubble. The three labeled data points show lower limits of the observationally inferred cloud density. All lines correspond to the evolution of a cloud in a time varying external gas component with pressure that increases with time as expected for G2 on its orbit into the center. With the exception of the dotted black line, tidal effects are neglected. The thick dashed line shows the theoretically expected density of G2 where it forms as a spherical cloud in the year 1995, neglecting tidal effects. For comparison, the dotted black line shows the mean density evolution of the numerical simulation CC01, also starting in 1995 (Section 6.1), where tidal effects are included. The thick blue line shows the density evolution where G2 starts at apocenter. Dashed red lines correspond to the evolution of a cloud that starts with a pressure that is a factor of 10 or 100 smaller at apocenter than required for pressure equilibrium. The solid red line shows the early expansion phase of an overpressured cloud with initial density that is a factor of 100 larger than the equilibrium density.

(A color version of this figure is available in the online journal.)

than the constant radius case due to the strong compression of the cloud at small orbital radii. To a good approximation, the cloud should then stay on a Keplerian orbit until pericenter. In the subsequent section, we will show that the actual evolution is more complex. The cloud might start in pressure equilibrium at apocenter. As soon as its internal sound crossing timescale exceeds the infall timescale it will, however, freeze out. At the same time, tidal effects will become important, stretching the cloud in the orbital direction while compressing it in the direction perpendicular to the orbit.

4.4. Pressure Confinement, Implosion, and Hydrodynamical Instabilities

As self-gravity is negligible, for a constant temperature T_c, the cloud will try to achieve a homogeneous density state in thermal pressure equilibrium with its surroundings. The shaded region in Figure 2 indicates the expected cloud density ρ_{equi} for the case of pressure equilibrium with the surroundings. The thick black line shows ρ_{equi}, adopting a hot gas temperature and density as given by Equations (2) and (3), with $T_c = 10^4$ K. The lower and upper boundaries correspond to $\eta_{hot} = 0.5$, $T_0 = 2 \times 10^8$ K and $\eta_{hot} = 1$, $T_0 = 3.5 \times 10^8$ K, respectively. Labeled black points show G2's estimated density, assuming its minor axis is marginally resolved. In this case, the cloud would have been in pressure equilibrium in 2003. ρ_{equi} increases strongly between 2003 and 2011. In contrast, the observations

reveal an increasing velocity gradient in the cloud as expected with decreasing orbital radius. Interestingly, the change in the velocity gradient is consistent with the assumption that G2's major axis remains roughly constant. The assumption of a minor axis close to the resolution limit then indicates that the cloud has frozen out with a constant density after 2003 that does not change significantly with time. The cloud's thickness in the unresolved direction perpendicular to its motion might, however, decrease continuously. In this case ρ_c would increase with time. The 2008 and 2011 points in Figure 2 then represent lower limits.

We unfortunately do not have detailed information about the cloud's structure prior to 2003. One can, however, investigate the question of whether a cloud like G2 could achieve pressure equilibrium in 2003 if it started with an arbitrary density at apocenter. The implosion of a gas clump that is imposed to a high pressure environment has been studied in detail by Klein et al. (1994). A shock front forms at the outer edge and sweeps up the cloud. It accelerates until the sum of the ram pressure of the shock $\rho_c v_s^2$ and the internal gas pressure $P_c = \rho_c c_c^2$ with c_c, the cloud's internal sound speed, is equal to the external pressure $P_{hot} = \rho_{hot} c_{hot}^2$, with c_{hot} the local sound speed of the surrounding gas, leading to an equilibrium shock velocity of

$$v_s^2 = \left(\frac{\rho_{hot}}{\rho_c} \right) c_{hot}^2 - c_c^2. \qquad (12)$$
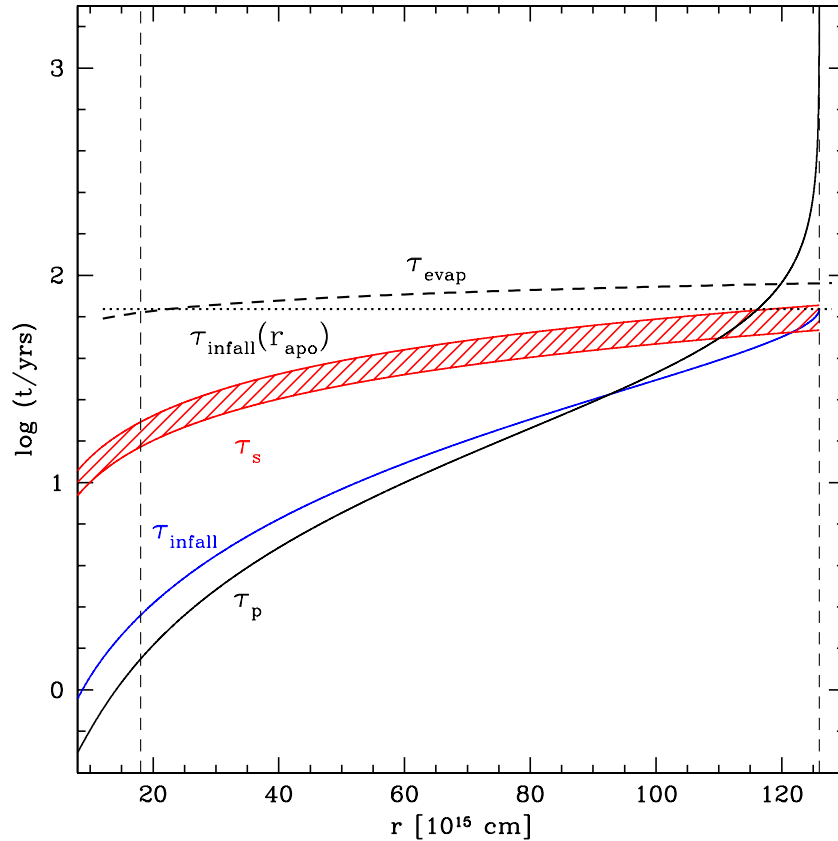
Figure 3. Various timescales are shown as functions of distance r from the SMBH that affect G2's evolution: the dynamical timescale τ_{dyn} (black, horizontal dotted line), the evaporation timescale τ_{evap} (black dashed line), the sound crossing timescale τ_s (shaded red region), adopting $\eta_{hot} = 1$ (upper limit) and $\eta_{hot} = 0.75$ (lower limit), respectively, the pressure timescale τ_p (black solid line), and the infall timescale τ_{infall} (blue solid line) that measures the time it takes G2 to reach pericenter from radius r. The horizontal dotted line shows the infall timescale at apocenter. The two vertical dashed lines correspond to the location of the apocenter and the location of G2 in 2011.3, respectively.

(A color version of this figure is available in the online journal.)

The cloud's crushing timescale is then

$$\tau_{cc} = \frac{R_c}{v_s} = \tau_s \left(\frac{P_{hot}}{P_c} - 1 \right)^{-1/2}, \qquad (13)$$

where we define $\tau_s = R_c/c_c$ as the cloud's sound crossing timescale, which is the timescale on which the cloud could react to external perturbations. For our typical parameters of a 10^4 K gas clump, in an environment described by Equations (2) and (3), this leads to

$$\tau_s = \left(\frac{3M_c}{4\pi c_c P_c} \right)^{1/3} = 13.2 \, \eta_{hot}^{-1/3} \left(\frac{r}{10^{16}\,\text{cm}} \right)^{2/3} \left(\frac{P_{hot}}{P_c} \right)^{1/3} \text{yr}. \qquad (14)$$

Figure 3 shows G2's sound crossing timescale (red shaded region) as a function of the orbital radius, assuming pressure equilibrium $P_{hot} = P_c$. Interestingly, close to apocenter, τ_s is equal to the infall timescale shown by the horizontal dotted line.

Equation (13) demonstrates that for $P_{hot} \gg P_c$ the crushing timescale of the cloud is much smaller than its sound crossing time and infall timescale. Starting close to apocenter, it should therefore implode long before reaching its current position. The dashed red lines in Figure 2 show the evolution of the mean density of such a cloud. For that, we integrated the evolution of the compression front, taking into account the time variation of $P_{hot}(r)$ as the cloud moves through the stratified environment with the pressure increasing with decreasing distance $r(t)$

from the SMBH. Assuming a constant cloud temperature, the evolution of the outer cloud radius is then given by $dR_c/dt = -v_s(t)$, where $v_s(t)$ depends on the orbital radius $r(t)$ according to Equation (12). Note that these clouds, when crossing the shaded area in Figure 2, continue to contract. Homogeneous clouds with these properties would be in pressure equilibrium with its surroundings and stable. In contrast, the imploding clouds, despite the fact that their volume averaged density is the same, contain an inner, low-pressure, and low-density core that is being swept up by a high-density, inward moving shell. Due to this core, they continue to contract.

As the high-density shock front is accelerated by a low-density gaseous environment, the cloud will be shredded by Rayleigh–Taylor instabilities that grow on a timescale of (Klein et al. 1994)

$$\tau_{RT} = \frac{\tau_{cc}}{(kR_c)^{1/2}}. \qquad (15)$$

The shortest wavelength or largest wavenumber k has the fastest growth rate. But Rayleigh–Taylor perturbations saturate in the nonlinear regime. As a result, the most destructive wavelength is given by $kR_c \approx 1$. The cloud should therefore be destroyed and mix with its surroundings on a timescale of the order of its crushing timescale. In summary, underpressured clouds, starting at apocenter, would disappear before reaching the presently observed position. If G2 came from apocenter, it would either be in pressure equilibrium with its surroundings or have even greater pressure.

Even if G2 is initially in pressure equilibrium, the pressure of the surrounding hot gas increases quickly on its way toward the SMBH. The cloud will be able to adjust as long as τ_s is short compared to the timescale τ_p on which the external pressure changes

$$\tau_p = \frac{1}{v_r d \ln P_{\mathrm{hot}}/dr} = \frac{r}{2v_r} \qquad (16)$$

with v_r the radial velocity of the cloud. The solid black line in Figure 3 shows $\tau_p(r)$, which for G2's orbit becomes smaller than τ_s quickly for $r \leqslant 10^{17}$ cm. Entering this region, the cloud will become a cold, low-pressure island within high-pressure surroundings and start imploding. The evolution of such a system is shown by the thick, blue line in Figure 2, where we have assumed that the implosion starts as soon as $\tau_p < \tau_s$. In 2003, G2's mean density should still be close to ρ_{equi}. At that point in the evolution, however, the timescale for the shock to completely crush the cloud has become smaller than the local infall timescale τ_{infall}, and its density now increases quickly. Here, we have neglected tidal shearing. As we will show in Section 6, tidal effects actually reverse the evolution, leading to a slightly decreasing density when the cloud approaches the inner regions of its orbit.

Within the framework of the "in situ" scenario discussed in Section 2, the cloud might have formed half-way between apocenter and the SMBH, e.g., in the year 1995, shortly before G2 was detected. The thick, black dashed line in Figure 2 shows the density evolution for this case. Due to G2's relatively high initial density, the velocity v_s of the inward moving shock is now slower and will not compress the cloud significantly within the next 12 years, while the pressure in the surroundings rises steeply. The cloud therefore evolves isochorically, in good agreement with the observations.

G2 might have started at apocenter in a high-density state with pressure that was greater than that in the surrounding gas. In this case, the cloud will first expand with a velocity that should be roughly equal to its sound velocity, trying to achieve pressure equilibrium with the environment. This expansion phase is shown by the solid red line in Figure 2. The subsequent evolution is complex and requires numerical simulations that will be discussed in Section 6.

5. PROBING THE TEMPERATURE AND DENSITY STRUCTURE OF THE CENTRAL HOT BUBBLE

G2 is a sensitive probe of the conditions in the central hot bubble. The early observations around 2002–2004, when the cloud is at a distance of $r \approx 5.5 \times 10^{16}$ cm provide especially important constraints on the density and pressure of the surrounding diffuse gas. In the following we will adopt the radial dependence of ρ_{hot} and T_{hot} as given by the Equations (2) and (3). In addition, we assume that the cloud is in pressure equilibrium with its surroundings in these early phases. As discussed in Section 4, a lower limit of the density of G2 in 2002–2008 is $\rho_c = 5 \times 10^{-19}$ g cm^{-3}. For a cloud temperature of $T_c = 10^4$ K, this implies $\rho_{\mathrm{hot,2002}} T_{\mathrm{hot,2002}} = 0.033 \times \rho_0 T_0 \geqslant 5 \times 10^{-15}$ K g cm^{-3} or

$$\rho_0 \times T_0 \geqslant 1.5 \times 10^{-13} \text{ g cm}^{-3} \text{ K}. \qquad (17)$$

If $\rho_0 \leqslant \eta_{\mathrm{hot}} \times 1.7 \times 10^{-21}$ g cm^{-3}, as inferred from the *Chandra* observations (Xu et al. 2006), $T_0 \geqslant 10^8/\eta_{\mathrm{hot}}$ K, which is in agreement with Equation (3) if $\eta_{\mathrm{hot}} = 0.5$. This would indicate that the fraction η_{hot} of X-ray luminosity, resulting

from unresolved stellar sources (Sazonov et al. 2012), is not dominant, as T_0 cannot be much larger than a few 2×10^8 K if the hot bubble is bound to the SMBH. Note that this conclusion is valid only if the cloud is roughly in pressure equilibrium with its surroundings in 2002, which is consistent with the numerical simulations that will be discussed in the subsequent section.

6. HYDRODYNAMICAL SIMULATIONS

In order to validate the results obtained from our analytical estimates and to investigate the future evolution of the cloud, we have conducted idealized hydrodynamical simulations. Here we discuss two-dimensional simulations and study the evolution of the cloud in the equatorial plane. Due to the dominant tidal effects, we do not expect that the results change significantly with three-dimensional simulations that will be presented in a subsequent paper.

The hydrodynamical equations were integrated with the help of PLUTO, version 3.1.1 (Mignone et al. 2007), which is a fully MPI-parallelized, high-resolution shock capturing scheme with a large variety of Riemann solvers. For all simulations shown in this article, we propagated the state vector with the two-shock Riemann solver, did a parabolic interpolation, and employed the third order Runge–Kutta time integration scheme. In these first simulations, we were interested in the evolution of the cloud in an idealized atmosphere with a smooth density and pressure distribution in concordance with observations, as discussed in Section 4. In order not to be dominated by the interaction of the cloud with disturbances of the convectively unstable atmosphere, we artificially stabilized the atmosphere. This was done by additionally evolving a passive tracer field ($0 \leqslant tr \leqslant 1$), which allowed us to distinguish those parts of the atmosphere that have interacted with the cloud ($tr \geqslant 10^{-4}$) from those that changed due to the atmosphere's inherent instability ($tr \leqslant 10^{-4}$). Those cells fulfilling the latter criterion were reset to the values expected in hydrostatic equilibrium. The boundary conditions were set to the values expected for hydrostatic equilibrium, enabling outflow but no inflow. The adiabatic index Γ of the cloud gas was set to one, which we consider a reasonable assumption, as the temperature of the cloud material is expected to be constant at 10^4 K due to the photoionization equilibrium in the radiation field of the surrounding stars (Gillessen et al. 2012). Our two-dimensional computational domain represents the orbital plane of the cloud, which initially starts in pressure equilibrium with the atmosphere except for simulation CC03, initially having an overpressure of a factor of 100. The corresponding parameters are summarized in Table 1. The cloud starts on the negative x-axis of the fixed Cartesian coordinate system with a spatial resolution of 7×10^{13} cm ranging from -1.3×10^{17} cm to 1.2×10^{16} cm in x-direction and -6.2×10^{16} cm to 2.5×10^{16} cm in y-direction. It orbits in a clockwise direction with the major axis parallel to the x-axis and the pericenter of the orbit on the positive x-axis. The black hole is located at the origin of our coordinate system. We neglect magnetic fields as well as feedback from the central source for the sake of simplicity and will give a more detailed analysis of the simulations and numerical tests of this approach in M. Schartmann et al. (2012, in preparation).

6.1. Model CC01: In Situ Formation of G2

Figure 4 shows the evolution of a cloud that was born as a spherical droplet in the year 1995 at a distance of 7.6×10^{16} cm. Dotted white contours depict the expected shape of the cloud
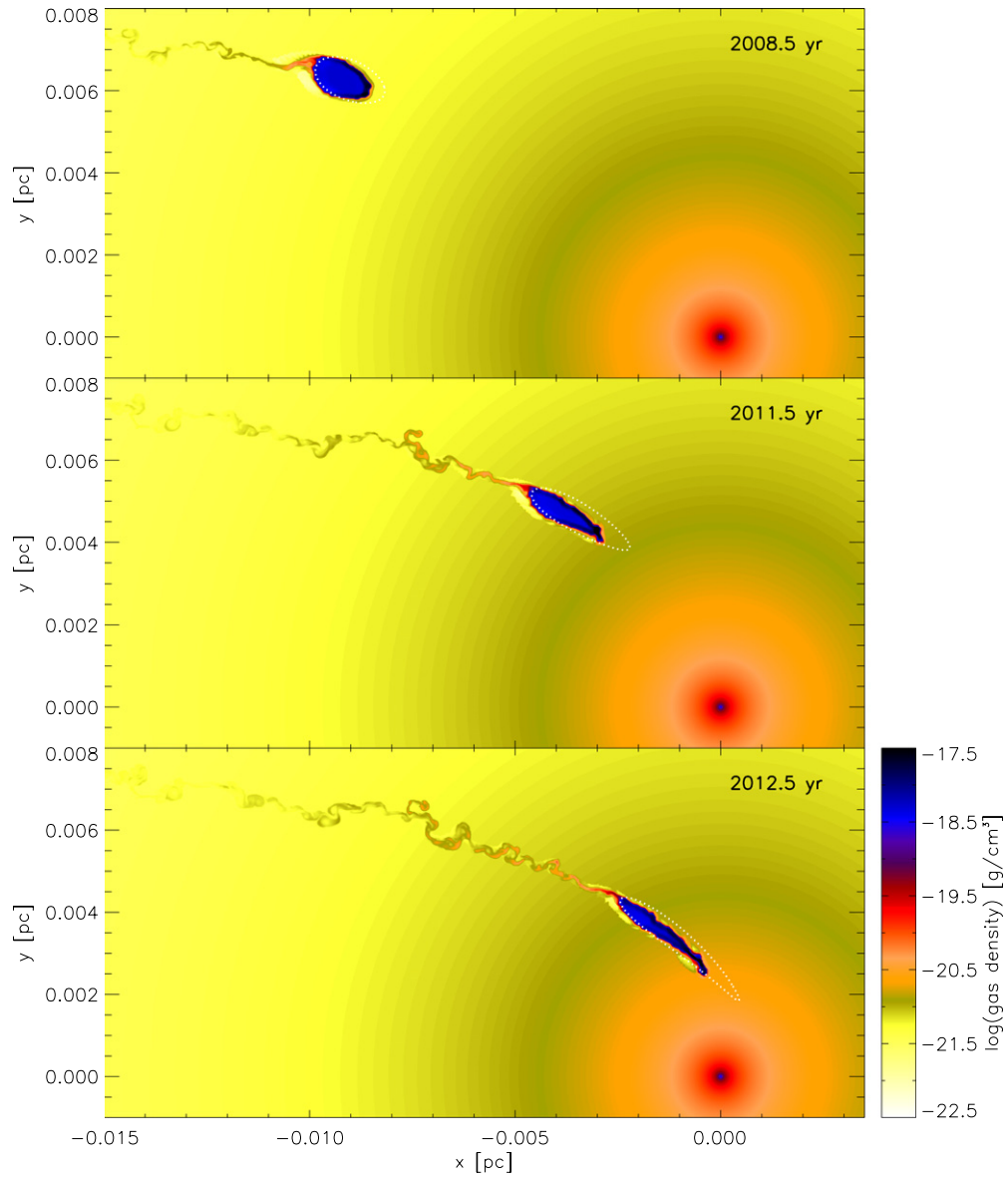
Figure 4. Early phases of the evolution of a cold gas cloud (model CC01) with a mass equal to G2 that starts in pressure equilibrium with its surroundings as a spherical clump in the year 1995. Colors correspond to the logarithm of gas density. White dotted contours correspond to a test particle simulation in which gas particles move on ballistic orbits.

(A color version of this figure is available in the online journal.)

Table 1
Parameters of the Hydrodynamical Simulations

	τ_0 [a] (yr AD)	ρ_{cloud} [b] (10^{-19} g cm^{-3})	R_{cloud} [c] (10^{15} cm)	x_{ini} [d] (10^{16} cm)	y_{ini} [e] (10^{16} cm)	v_{ini}^x [f] (km s^{-1})	v_{ini}^y [g] (km s^{-1})
CC01	1995.5	6.21	1.87	−7.22	2.21	794.59	48.45
CC02	1944.6	2.24	2.63	−12.59	0.0	0.0	167.29
CC03	1944.6	223.64	0.57	−12.59	0.0	0.0	167.29
SS01	1927.2	1.42	11.8	−15.80	0.0	0.0	125.00

Notes. CC refers to simulations of the cloud scenario and SS to those of the spherical shell scenario.
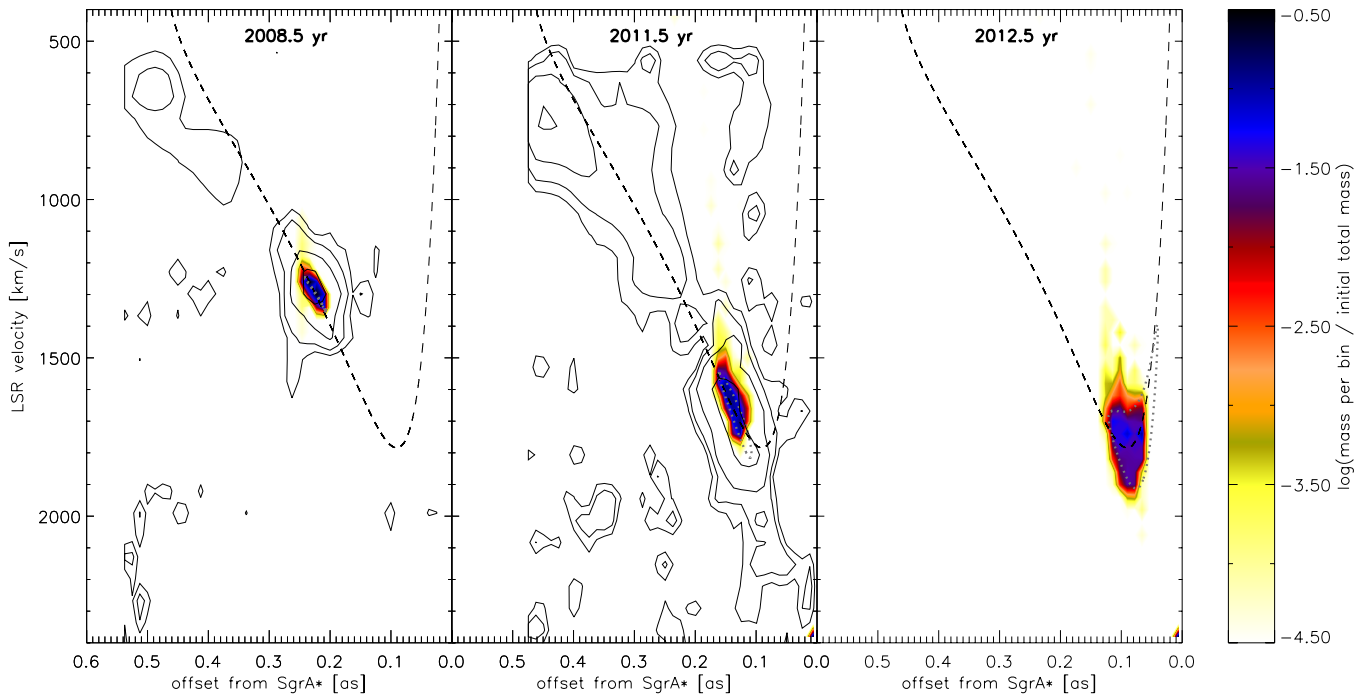[a] Start time of the simulation.
[b] Initial density of the cloud.
[c] Initial radius of the cloud.
[d] Initial x-position of the cloud.
[e] Initial y-position of the cloud.
[f] Initial x-velocity of the cloud.
[g] Initial y-velocity of the cloud.

Figure 5. Position vs. line-of-sight velocity map of the "in situ" formation model CC01 (see also Figure 2 of Gillessen et al. 2012), which corresponds to a cloud that formed in 1995. The contours show the Brγ emission of G2, obtained with SINFONI on the Very Large Telescope (Gillessen et al. 2012). Colors correspond to the total mass of gas as predicted by the simulation in each position–velocity bin, with the values given by the color bar. The dashed line shows the ballistic orbit of a point particle in the gravitational potential of the SMBH, centered on G2. The dotted lines show the distribution where each gas element of the cloud moves on a ballistic orbit. In 2008.5 the cloud is still compact. Over the next 3 years its develops a strong velocity shear. Overall, the calculations are in excellent agreement with the observations. The predicted structure of G2 in the PV diagram for the year 2012.5 is shown in the right panel.

(A color version of this figure is available in the online journal.)

from a collisionless test particle simulation, if each gas particle would move on a ballistic orbit within the gravitational potential of the SMBH. In 2008.5 the hydrodynamical interaction with its surroundings is still minor, and the cloud's structure follows the outer contour of the test particle simulations very well. In this early phase, the cloud is already developing an elongated structure due to tidal effects. Ram pressure stripping at the outer edge also generates a trailing tail of gas that is dispersed by Kelvin–Helmholtz instabilities. The mass loss is, however, negligible. In 2011.5 and 2012.5 the cloud has become significantly more elongated. Ram pressure effects are now more clearly visible at the front side, which is falling behind the ballistic orbits. The dotted black line in Figure 2 shows the mean density evolution as a function of the orbital radius. In agreement with our analytical estimates (dashed black line in Figure 2), the cloud's density does not change significantly between 1995 and 2011, as the crushing timescale for an object that starts in 1995 is longer than its infall timescale. While the mean density in the idealized model is continuously rising due to compression, it actually decreases slowly in the numerical simulation due to the tidal shearing along the orbit. This might be partly an artifact of the two-dimensional simulations; it must be confirmed by future three-dimensional models.

Figure 5 compares the structure of the simulated cloud in the PV diagram with the observations. In the year 2008.5 the cloud is still compact. In 2011.5 it develops a strong shear that follows the center-of-mass, ballistic orbit (dashed line). Overall, the structure of the simulated cloud in the PV diagram is in excellent agreement with the observations (contours). The predicted structure and kinematics in 2012.5 are shown in the third panels of Figures 4 and 5, when the cloud has reached the point of maximum line-of-sight velocity. In the PV diagram

the cloud's contours still do not deviate significantly from a ballistic orbit, shown by the dotted lines.

Figure 6 shows G2's structure for the "in situ" scenario during and after pericenter passage. At pericenter, the cloud will be tidally stretched into a long, curved filament. As discussed in Section 4.3, the hydrodynamical drag is not strong enough to remove a large fraction of the cloud's kinetic energy. As a result, the bulk of the gas again is moving out to large distances. Ram pressure at the head, however, has removed a substantial amount of kinetic energy and angular momentum, forcing the front of the filament to fall into the unresolved inner accretion zone of Sgr A* (the upper panel). The middle panel of Figure 6 shows that on its way outward the gas is first compressed both by the negative divergence of the velocity field and by ram pressure. Large Kelvin–Helmholtz eddies are now visible at the inner edge, facing the SMBH, that begin to destroy the cloud, leading to several narrow gas streams that fall into Sgr A*. In 2050.5 the cloud has completely dissolved, generating a narrow, dense stream of cold gas that feeds the SMBH.

### 6.2. Model CC02: Formation of G2 at Apocenter

We have argued in Sections 2 and 3 that it is more likely for the cloud to have started in the clockwise rotating stellar disk, which agrees with the cloud's orbital plane and which has an inner edge equal to its apocenter. Figure 7 shows the evolution of an initially spherical, cold gas droplet in pressure at equilibrium at apocenter. Initially, the cloud remains in pressure at equilibrium with its surrounding, in agreement with the analytical estimate (the blue line in Figure 2). However, even in these early phases tidal effects begin to reshape the cloud. The upper panel of Figure 8 shows the characteristic velocity field in the cloud at
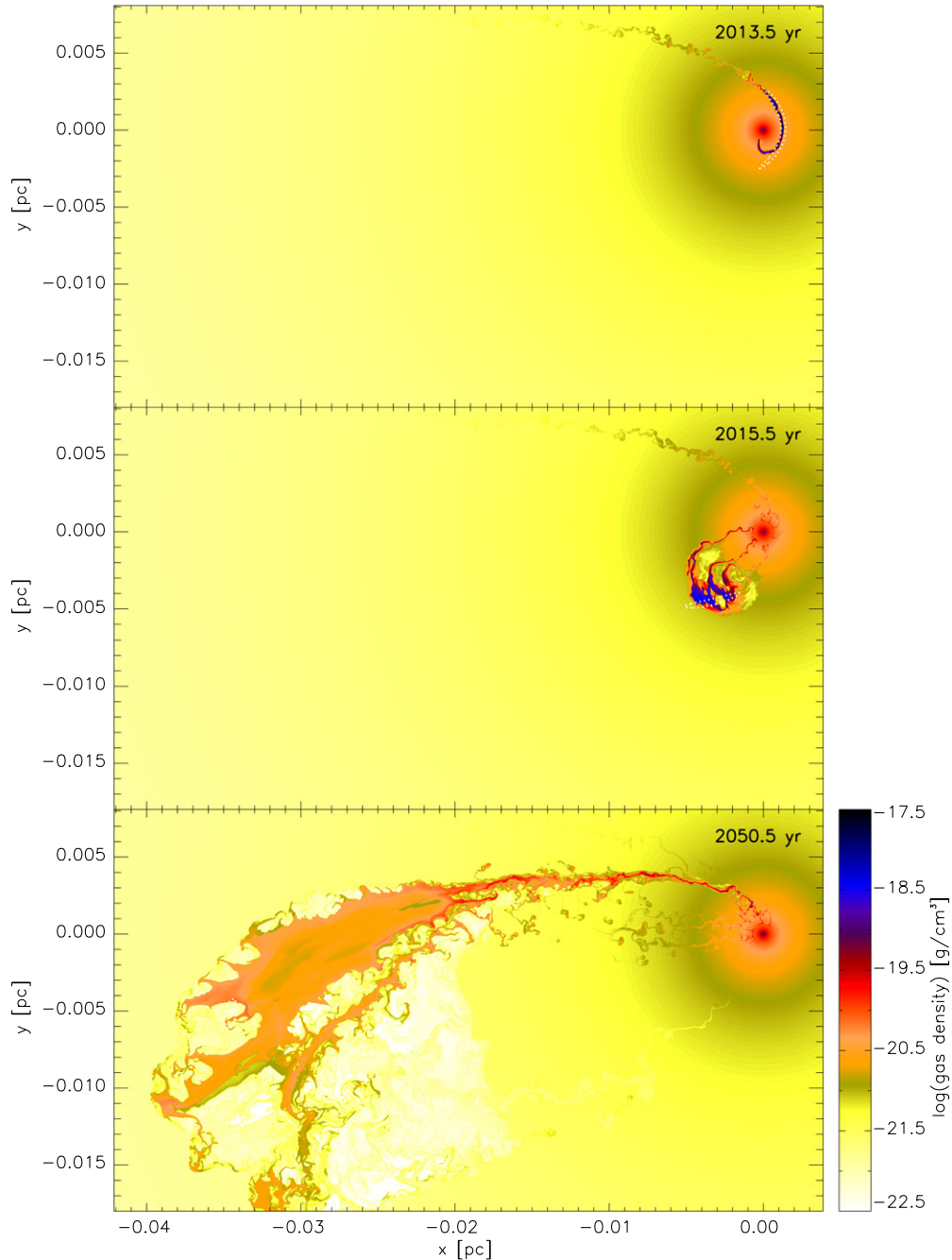
Figure 6. Late phases of the evolution of model CC01. In the year 2050, the cloud has broken up into a long filament that feeds Sgr A*.
(A color version of this figure is available in the online journal.)

1980.6 after subtracting its center-of-mass motion (large black arrow). The mean cloud density is 2×10^{-19} g cm^{-3}, which is in agreement with our analytical estimates. However, despite the fact that the cloud is still at a distance of 10^{17} cm, the strong tidal shear has already generated a strong internal velocity field that pushes material outward along the orbit, while at the same time compressing the cloud perpendicular to it. The surrounding gas pressure, even in combination with the ram pressure, is not strong enough to stop this flow. Note also that the cloud has developed a density gradient due to ram pressure compression at the front. The lower panel of Figure 8 shows the cloud at 2003.6, when it is at a distance of 5.3×10^{16} cm. Its mean density has increased to $\rho_c = 10^{-18}$ g cm^{-3}, which is in agreement with the observationally inferred cloud density (Figure 2). It is, however, in disagreement with our analytical estimates, which predicted higher compression if tidal effects are neglected. This is due to the fact that at this stage tides have turned the cloud into a long filament. The situation has become even more extreme in 2011.6 (the middle panel of Figure 7) where the filament has grown to a length of 3×10^{16} cm, which is much longer than the observationally inferred length of $\leqslant 3 \times 10^{15}$ cm. Note that the filament is distorted by Kelvin–Helmholtz instabilities as a result of its interaction with the diffuse surrounding. In 2012.6 (the lower panel of Figure 7), these instabilities have become nonlinear and begin to break up the system into a string of clumps that begin to fall into the SMBH. The PV diagram shown
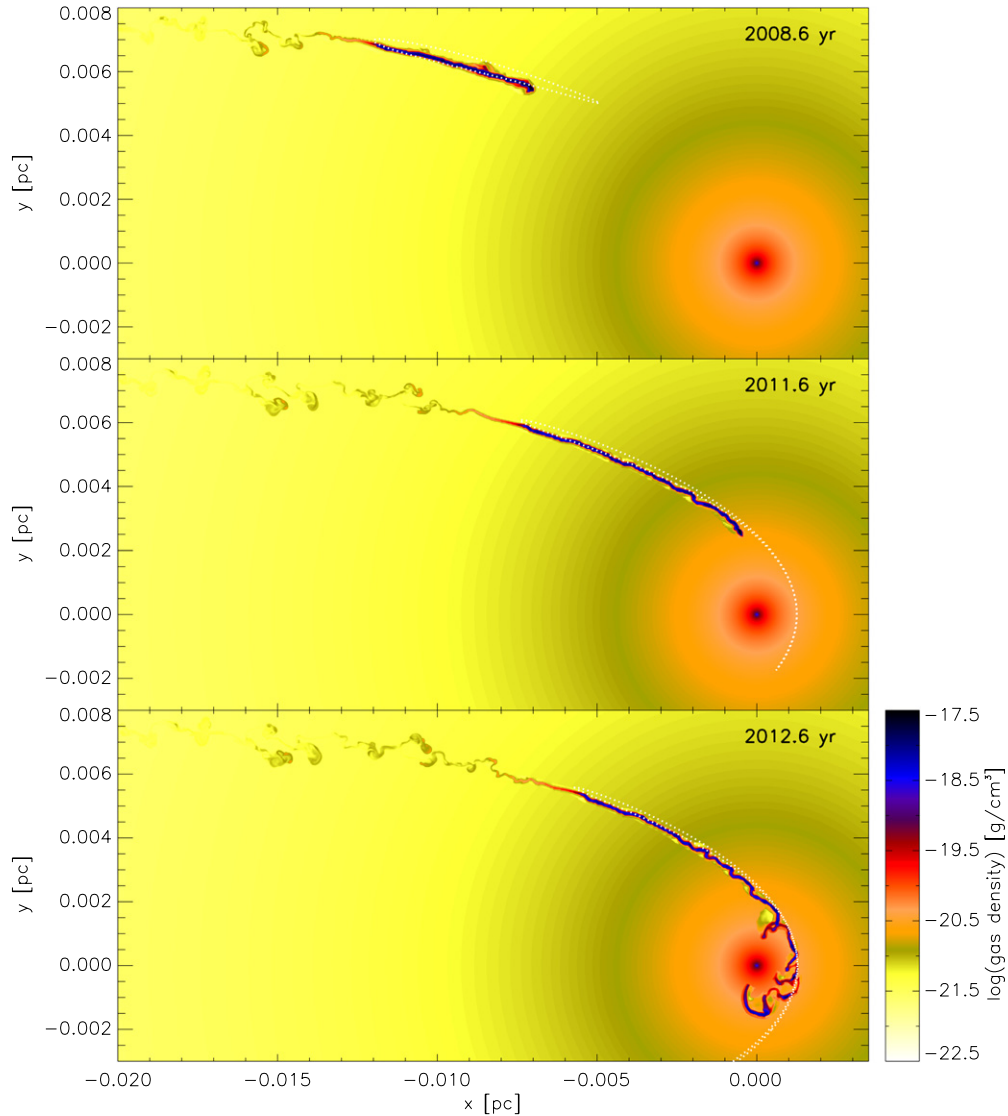
Figure 7. Same as Figure 4 for model CC02. Now, the cloud starts in pressure equilibrium at apocenter.
(A color version of this figure is available in the online journal.)

in Figure 9 confirms that the structure is much too elongated compared to the observations.

6.3. Model CC03: An Overpressured High-Density Cloud at Apocenter

We argued in (Section 4) that a cloud that has pressure much greater than its surroundings will expand. The detailed evolution is, however, difficult to predict analytically. We therefore show in Figure 10 the evolution of a clump that started at apocenter with an initial density that is a factor of 100 larger than the equilibrium density ρ_{equi}. The cloud initially expands, but the expansion does not stop as soon as the mean cloud density has become equal to ρ_{equi} due to the outward directed velocity field. The cloud overshoots this equilibrium point, and its density and pressure drop further, with the cloud forming a very extended structure that is now subject to the strong tidal forces as shown in Figure 10. As in the previous case, the PV diagram (Figure 11) is not at all in agreement with the observations. This confirms our previous conclusion that, if G2 is a cloud, it started its journey into the center close to pressure at equilibrium with its surroundings.

6.4. Model SS01: The Spherical Shell Model

Up until now, we have assumed that G2 is an isolated, small Earth mass cloud that formed either close to the location of first detection or at apocenter. It might, however, be part of a larger structure. The observations (Figure 2 of Gillessen et al. 2012; contours in the PV diagrams, e.g., Figure 5) indeed show extended emission downstream of G2, with a brighter area at the end that is offset with respect to G2's orbit with a line-of-sight velocity difference of order $500 \, km \, s^{-1}$. We have tried to generate an initial condition at apocenter that could reproduce these observations and found that a surprisingly simple symmetric shell of gas in the orbital plane with a tangential velocity of $125 \, km \, s^{-1}$, similar to G2's initial velocity, an outer radius of $1.2 \times 10^{16} \, cm$, and a thickness of $3 \times 10^{15} \, cm$ can well reproduce the observations (Table 1). Its gas density $\rho_c = 1.42 \times 10^{-19} \, g \, cm^{-3}$ is given by the requirement that it is in pressure equilibrium with its surrounding. Such a structure could have been produced either by the dusty wind shells of massive stars, an explosion, or an object that crossed the plane of the stellar disk at apocenter. Figure 12 shows the evolution of the shell. G2 in this case represents its leading head, which
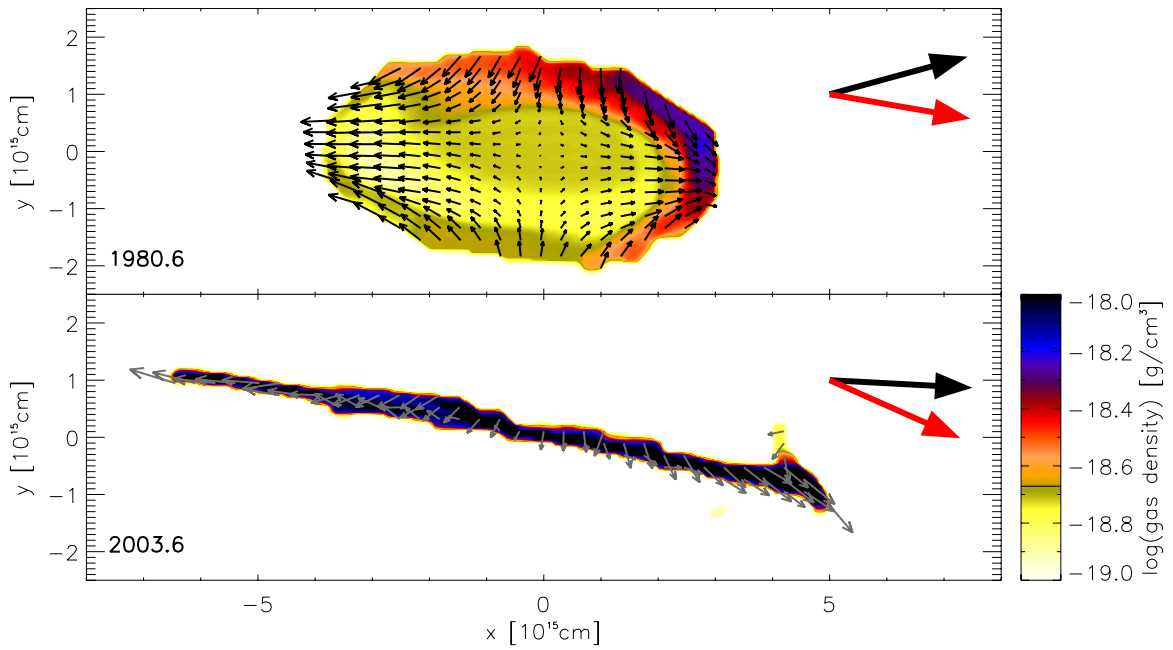
Figure 8. Density distribution and velocity field in the cloud in model CC02 that starts in pressure equilibrium at apocenter. The upper panel shows the early cloud structure in the year 1980.6. The two large vectors show the radial direction toward the SMBH (red) and the mean orbital velocity vector (black) of the cloud, respectively. The velocity field represents the internal velocity of the cloud's gas after subtracting the center-of-mass velocity (large black arrow). The size of the velocity vectors scales linearly with velocity. As reference, the large arrows in the upper and lower panels correspond to a velocity of 485 km s^{-1} and 1135 km s^{-1}, respectively. The cloud is compressed perpendicular to its orbit and tidally sheared along its orbit. Due to ram pressure a high-density shell is visible at the upstream front of the cloud. The lower panel shows the structure in the year 2003.6. The cloud has been torn apart into a long spaghetti-like filament.

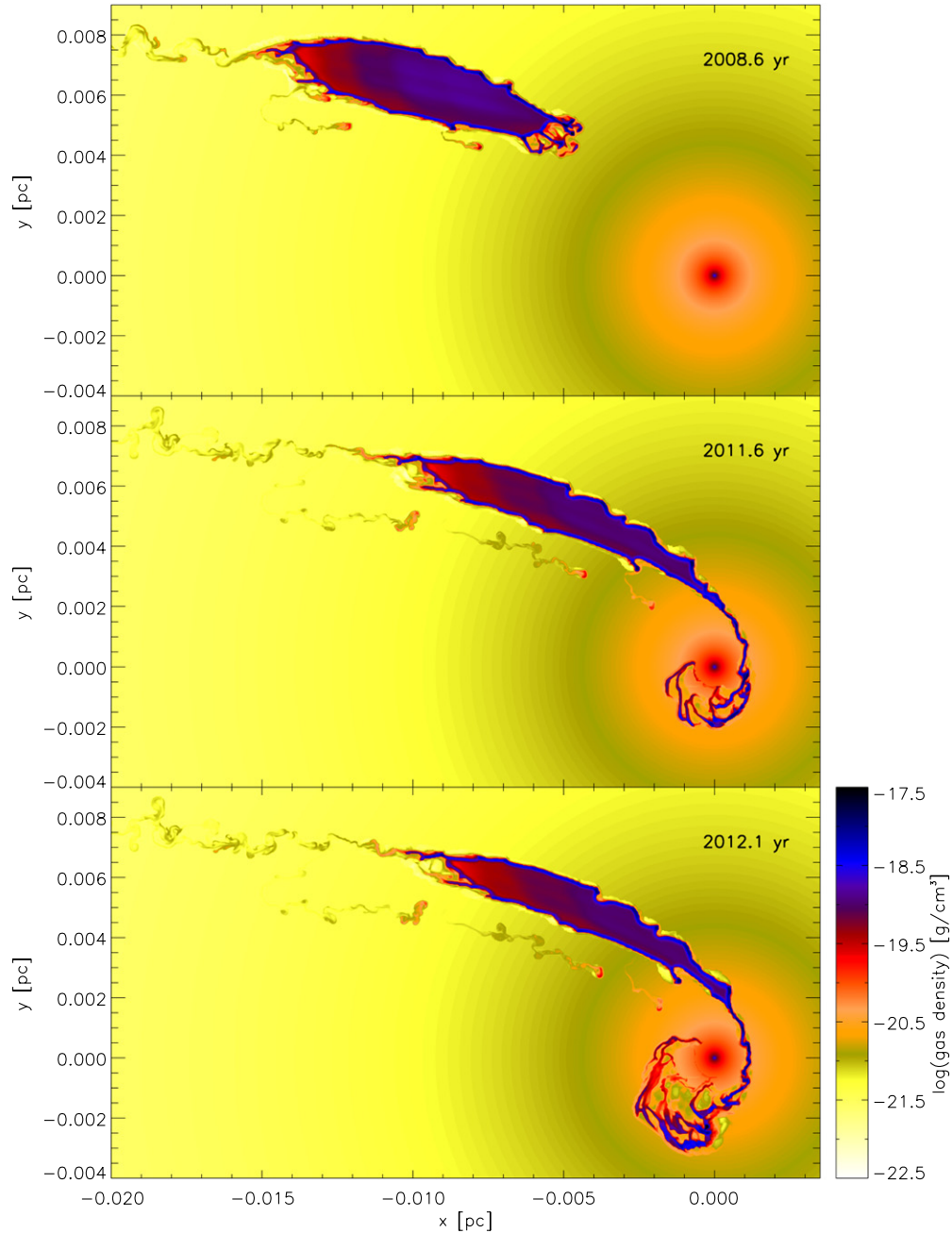(A color version of this figure is available in the online journal.)
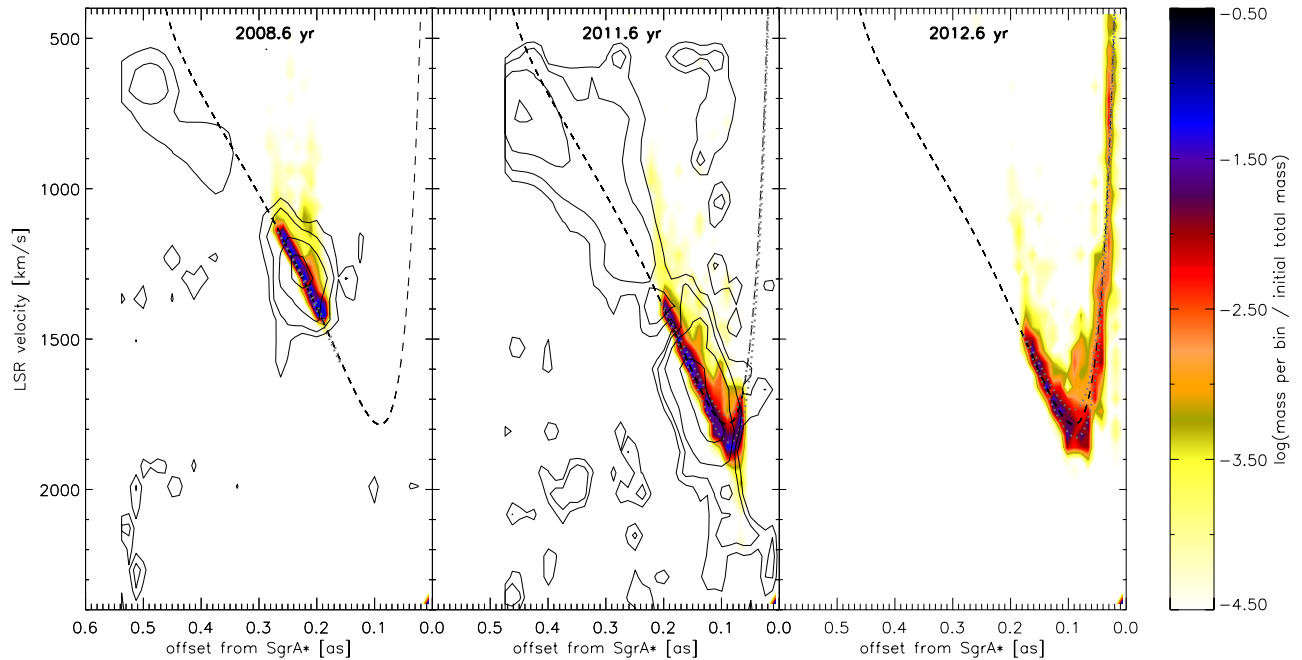
Figure 9. Position–velocity diagram of model CC02, a cloud that starts at apocenter.
(A color version of this figure is available in the online journal.)

is being compressed into a spheroidal clump as a result of the converging, radial inflow. Interestingly, the projection of this distorted shell along the line of sight also generates a second high surface density region that is connected to G2 by low surface density gas. This is clearly shown in the shell's PV diagram (Figure 13). Note that this second bright point is also offset with respect to G2's orbit (dashed line) by ∼500 km s^{-1}, as observed.

7. DISCUSSION AND CONCLUSIONS

We investigated the origin and evolution of the small gas cloud G2 that has been detected approaching the Galactic SMBH on a highly eccentric orbit. The cloud has an observationally inferred density and temperature that during the first years of detection around 2003 indicate that it was in pressure equilibrium with its surrounding. Our analytical estimates and numeric simulations
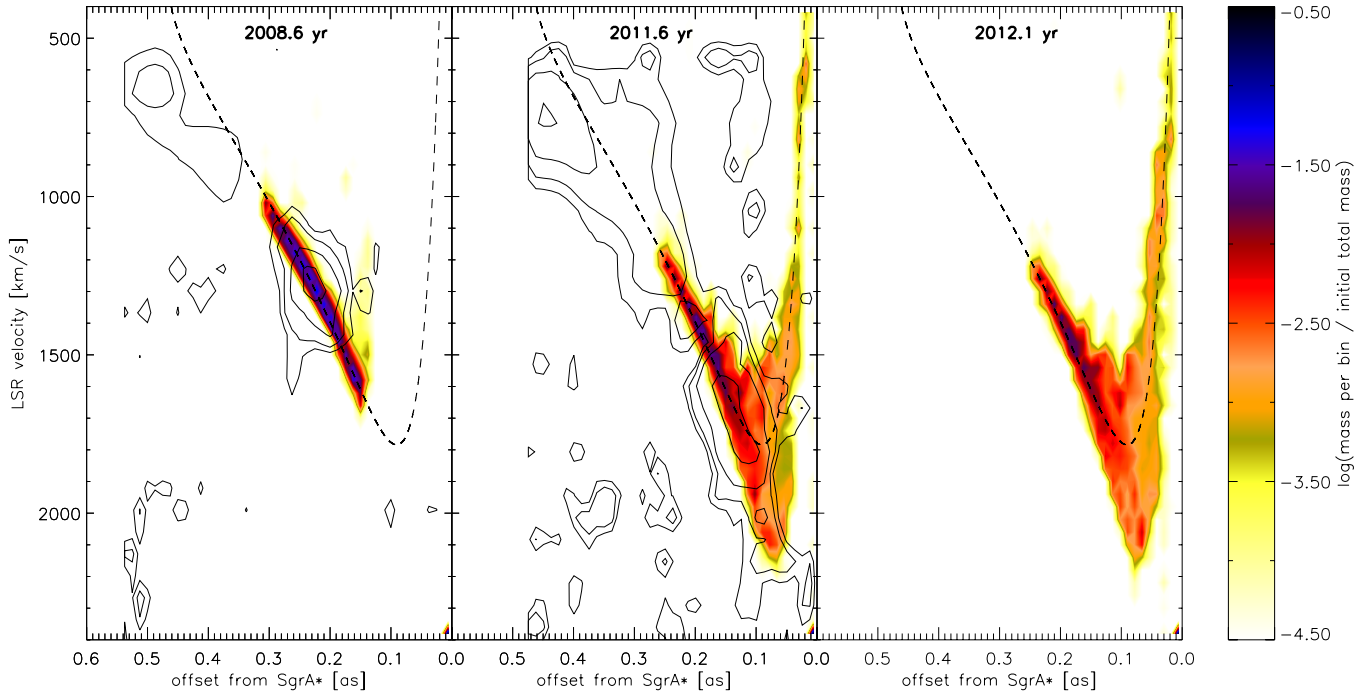
Figure 10. Evolution of model CC03, a cloud that starts at apocenter with a density and pressure that are a factor of 100 larger than those of its surroundings. Due to the resulting expansion, the cloud evolves into a large clump with internal pressure that is significantly lower than that of its surroundings.

(A color version of this figure is available in the online journal.)

show that it must have formed close to pressure equilibrium. A cloud with a significant lower pressure would be destroyed by implosion, while a highly overpressured cloud would go through a phase of rapid expansion, forming a diffuse, extended, and tidally elongated structure that is not in agreement with the observations. The "in situ" cloud scenario, which assumes that the cloud formed as a spheroidal clump in pressure equilibrium in the year 1995, shortly before it was detected, provides an excellent match to all the observations, dating back to 2002 until today. In this case, our numerical simulations indicate that the cloud will be tidally stretched into a very elongated filament until 2013.5 and shortly after pericenter passage will begin to lose gas as a result of Kelvin–Helmholtz instabilities. This gas might fall into the inner accretion zone of Sgr A*, forming a hot

luminous accretion disk. Over the next 80 years, the debris of the tidally destroyed cloud will fuel the SMBH, perhaps leading to an extended period of nuclear activity.

The main caveat of the "in situ" model is the fact that we have not been able to identify any physical mechanism that could have formed G2 in 1995. We did not find any known star that was close to its birthplace at that time. In addition, the cloud could also not have been formed by a cooling instability of the hot gas, as its cooling timescale is much longer than the dynamic timescale (Burkert & Lin 2000).

It is intriguing that the assumption of G2 having formed at apocenter leads to several interesting correlations that should be reproduced by any theoretical model of its formation. G2's orbital plane coincides with the plane of the clockwise rotating
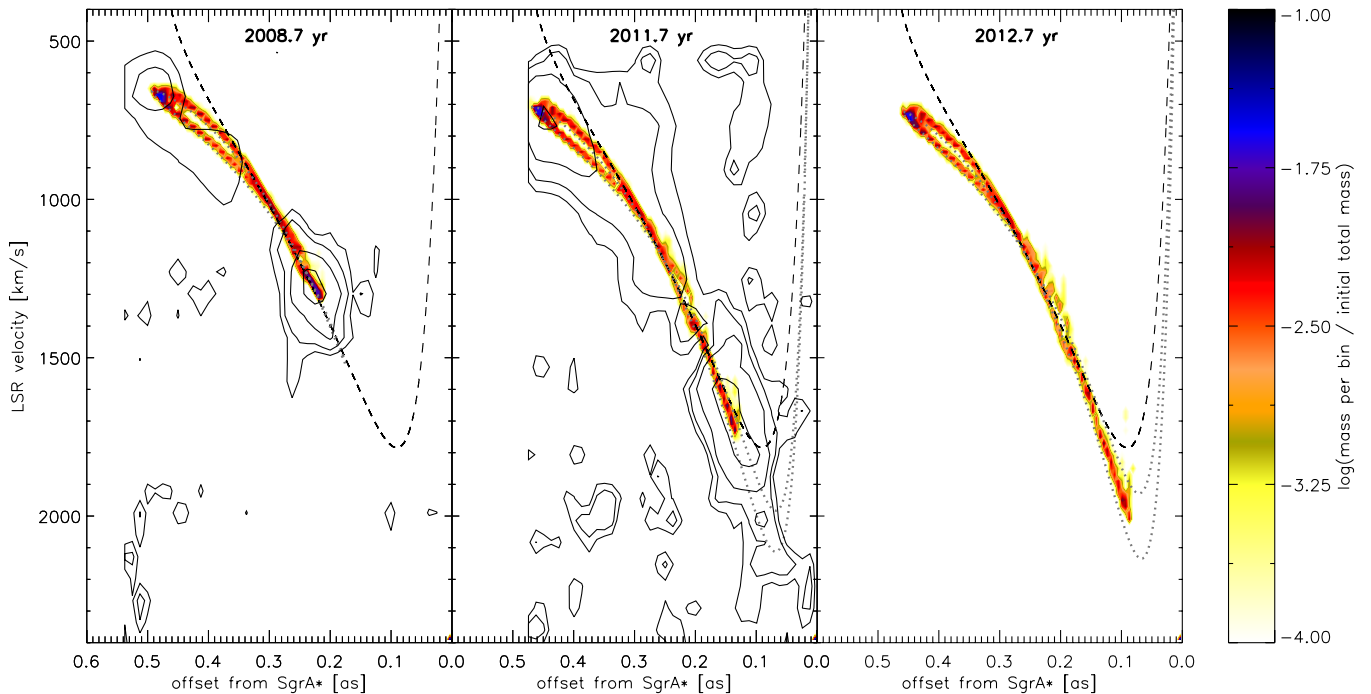
Figure 11. PV diagram of model CC03.
(A color version of this figure is available in the online journal.)
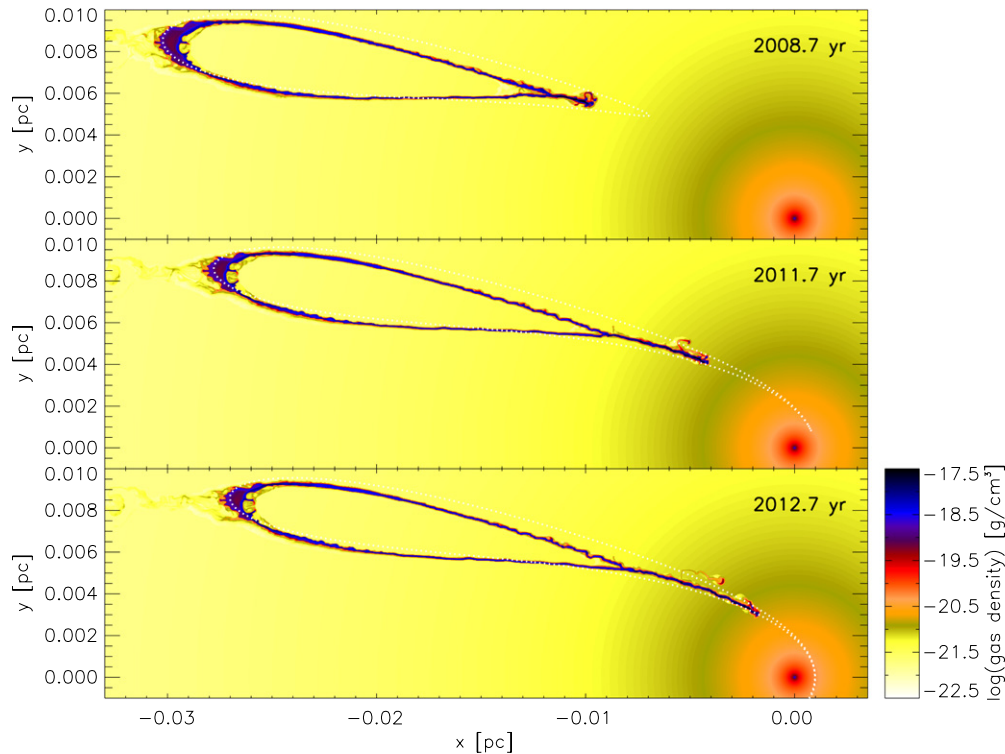
Figure 12. Evolution of the spherical shell model SS01, which assumes that gas is initially distributed in a ring-like structure at apocenter.
(A color version of this figure is available in the online journal.)

stellar disk, and its apocenter agrees with the inner disk edge. In addition, G2's sound crossing timescale, evaporation timescale, and infall timescale are all equal at apocenter. If this is not a coincidence, it provides several important constraints on its formation. First of all, G2 obviously did not form very recently (e.g., 1995) through some condensation processes, but it instead came from apocenter. It also means that G2 has been

in pressure equilibrium at apocenter, either as a result of its formation or due to readjustment. It is reasonable to assume that a cloud that is subject to distortions when interacting with a turbulent environment can only maintain coherence if it reacts and readjusts to those distortions. This requires that the cloud's sound crossing timescale, which is the timescale on which information is transported through the cloud, is smaller than

Figure 13. PV diagram of model SS01, which forms two bright regions of emission with diffuse material in between, similar to the observations.
(A color version of this figure is available in the online journal.)

the timescale of the perturbation. Clouds that cannot react will break up into subunits that are smaller than this characteristic timescale. The origin of these perturbations has not been clear until now. The inner hot bubble is probably highly turbulent and might even be convective. For a Kolmogoroff spectrum, the largest fluctuations, which are of the order of the size of the region and which interact with the cloud on timescales of the order of the infall timescale, would dominate and might regulate its size. In this case, G2 might represent a piece of a larger dusty cold region that disintegrated into smaller clumps by its interaction with the turbulent environment. As the timescale for such a region to break up is at least equal to the infall timescale, the cold gas inside G2 must be older than that. G2 should then have completed at least one full orbit. The massive progenitor cloud might already have been on a highly eccentric orbit at that time. Another possibility is that it was on a circular orbit within the stellar disk region, where it experienced a collision or violent interaction, e.g., with a stellar wind shell. This destroyed the cloud while at the same time deflected some of its parts onto highly eccentric orbits like G2.

One of the problems with all formation scenarios that start at apocenter is the fact that G2 will become very elongated with a strong velocity gradient around 2011 that is not in agreement with the observations. As our simulations show, one possible solution is that G2 is actually part of a larger shell. This scenario could explain the observed extended tail of lower surface brightness Brγ emission that is seen on about the same orbit as that of G2. The shell's origin is not clear. It might represent a clumpy wind shell, ejected from one of the luminous blue variable or Wolf–Rayet stars in the stellar disk. We investigated which of the known high-mass stars in the stellar disk was close to G2's apocenter in the year 1944 and found one candidate, S91, which appears to be an O6.5II star with a mass-loss rate of order $(1 \pm 0.5) \times 10^6 \, M_\odot \, \mathrm{yr}^{-1}$ and a wind velocity of $2000 \pm 500 \, \mathrm{km \, s}^{-1}$ (J. Puls & R. Kudritzki 2011, private communication). Winds of this kind are usually

believed to generate hot plasma with temperatures of the order of a few 10^7 K (Hall et al. 1982; Cuadra et al. 2005). Whether a cooling instability in the expanding wind bubble could also have generated a ring of cold gas is not yet clear.

If the cloud scenario of G2 fails, we are left with the possibility that G2 is actually the visible diffuse gas atmosphere of an unresolved, dense object in its center (compact source scenario; Murray-Clay & Loeb 2012). This would keep the cloud spheroidal, despite the external gravitational force of the SMBH, first because gas is continuously replenished from the probably spherical radial outflow, and second because the gravitational force of the central object inside the Roche volume can balance the destructive and deforming gravitational force of the SMBH. A crucial test of this scenario is whether it can explain the close agreement between the sound crossing, evaporation, and infall timescales that we discussed earlier. In this case, one also would expect a tail of stripped material, trailing G2. Its structure and especially its velocity distribution might, however, differ significantly from the shell scenario. For example, it is not clear whether its downstream end would be bright. In addition, it is unlikely that the trailing stripped gas will have the observed offset toward large infall velocities compared to the orbital velocity. We would instead expect smaller infall velocities due to the deceleration by the ram pressure, which is not observed. Detailed observations of the diffuse environment of G2 and additional numerical simulations would be helpful in distinguishing between the cloud and compact source scenario.

We have presented and discussed a set of simplified simulations, adopting a hydrostatic atmosphere and an isothermal cloud. These simulations already reveal a very complex, nonlinear evolution. Future papers should add the effects of compressional heating of the cloud, especially close to pericenter, where Gillessen et al. (2012) estimate compression to significantly increase the temperature and by that the luminosity of the cloud. First test simulations demonstrate, however, that this effect does not significantly alter the cloud's evolution as the

gravitational force of the SMBH close to pericenter is much stronger than the increase in gas pressure due to tidal heating. After pericenter the cloud material will actually cool again due to expansion. It is also important to investigate the effects of gas evaporation and magnetic fields. In the long run one should replace the currently hydrostatic atmosphere with a turbulent and probably convective, inhomogeneous and rotating hot gas bubble that might strongly affect the cloud evolution.

The problem of the origin and evolution of the tiny gas cloud G2 falling into the accretion zone of Sgr A* represents an exciting challenge for numerical and theoretical models of the complex multi-phase gas physics in the Galactic center. We are in a unique situation in which theoretical models and numerical simulations of G2's evolution will be tested directly by observations within the next couple of years. For the next decades G2's journey through the Galactic nucleus and its evolution will provide detailed information about this fascinating and extreme environment of the Milky Way and the processes that feed its central SMBH.

REFERENCES

Alexander, R. D., Smedley, S. L., Nayakshin, S., & King, A. R. 2012, MNRAS, 419, 1970
Alig, C., Burkert, A., Johansson, P. H., & Schartmann, M. 2011, MNRAS, 412, 469
Baganoff, F. K., Bautz, M. W., Brandt, W. N., et al. 2001, Nature, 413, 45
Baganoff, F. K., Maeda, Y., Morris, M., et al. 2003, ApJ, 591, 891
Bartko, H., Martins, F., Fritz, T. K., et al. 2009, ApJ, 697, 1741
Burkert, A., & Lin, D. 2000, ApJ, 537, 270
Burkert, A., & Tremaine, S. 2010, ApJ, 720, 516
Bonnell, I. A., & Rice, W. K. M. 2008, Science, 321, 1060
Bower, G. C., Wright, M. C. H., Falcke, H., & Backer, D. C. 2003, ApJ, 588, 331
Chevalier, R. A. 1992, ApJ, 397, L39
Clênet, Y., Roun, D., Gratadour, D., et al. 2005, A&A, 439, 9
Coker, R., & Melia, F. 1997, ApJ, 488, L149
Cowie, L. L., & McKee, C. F. 1977, ApJ, 211, 135
Cuadra, J., Nayakshin, S., & Martins, F. 2008, MNRAS, 383, 458
Cuadra, J., Nayakshin, S., Springel, V., & Di Matteo, T. 2005, MNRAS, 360, L55
Cuadra, J., Nayakshin, S., Springel, V., & Di Matteo, T. 2006, MNRAS, 366, 358
Field, G. B., Goldsmith, D. W., & Habing, H. J. 1969, ApJ, 155, L49
Genzel, R., Eisenhauer, F., & Gillessen, S. 2010, Rev. Mod. Phys., 82, 3121
Genzel, R., Schödel, R., Ott, T., et al. 2003, ApJ, 594, 812
Ghez, A. M., Salim, S., Hornstein, S. D., et al. 2005, ApJ, 620, 744
Ghez, A. M., Salim, S., Weinberg, N. N., et al. 2008, ApJ, 689, 1044
Gillessen, S., Eisenhauer, F., Trippe, S., et al. 2009, ApJ, 692, 1075
Gillessen, S., Genzel, R., Fritz, T. K., et al. 2012, Nature, 481, 51
Goldwurm, A. 2011, in ASP Conf. Ser. 439, The Galactic Center: a Window to the Nuclear Environment of Disk Galaxies, ed. M. R. Morris, Q. D. Wang, & F. Yuan (San Francisco, CA: ASP), 391
Gültekin, K., Richstone, D. O., Gebhardt, K., et al. 2009, ApJ, 698, 198
Hall, D. N. B., Kleinmann, S. G., & Scoville, N. Z. 1982, ApJ, 260, L53
Hawley, J. F., & Balbus, S. A. 2002, ApJ, 573, 738
Heckman, T. M., Kauffman, G., Brinchmann, J., et al. 2004, ApJ, 613, 109
Heitsch, F., & Putman, M. E. 2009, ApJ, 698, 1485
Hobbs, A., & Nayakshin, S. 2009, MNRAS, 394, 191
Johnson, B. M., & Quataert, E. 2007, ApJ, 660, 1273
King, A. R., & Pringle, J. E. 2007, MNRAS, 377, L25
Klein, R. I., McKee, C. F., & Colella, P. 1994, ApJ, 420, 213
Koo, B. C., & McKee, C. F. 1992, ApJ, 388, 93
Kormendy, J., Bender, R., & Cornell, M. E. 2011, Nature, 469, 374
Koyama, K., Maeda, Y., Sonobe, T., et al. 1996, PASJ, 48, 249
Koyama, K., Senda, A., Murakami, H., & Maeda, Y. 2003, Chin. J. Astron. & Astrophys., 3, 297
Koyama, K., Takikawa, Y., Hyodo, Y., et al. 2009, PASJ, 61, 255
Krabbe, A., Genzel, R., Drapatz, S., & Rotaciuc, V. 1991, ApJ, 382, L19
Kwak, K., Henley, D. B., & Shelton, R. L. 2011, ApJ, 739, 30
Loeb, A. 2004, MNRAS, 350, 725
Marrone, D. P., Moran, J. M., Zhao, J.-H., & Rao, R. 2007, ApJ, 654, L57
Martins, F., Genzel, R., Hillier, D. J., et al. 2007, A&A, 468, 233
Melia, F. 1992, ApJ, 387, L25
Melia, F., Jokipii, J. R., & Narayanan, A. 1992, ApJ, 395, L87
Mignone, A., Bodo, G., Massaglia, S., et al. 2007, ApJS, 170, 228
Murray, S. D., & Lin, D. N. C. 2004, ApJ, 615, 586
Murray-Clay, R. A., & Loeb, A. 2012, arXiv:1112.4822
Najarro, F., Krabbe, A., Genzel, R., et al. 1997, A&A, 325, 700
Narayan, R., & Yi, I. 1994, ApJ, 428, L13
Narayan, R. 2002, in Lighthouses of the Universe, ed. M. Gilfanov et al. (Berlin: Springer), 405
Narayan, R., Igumenshchev, I., & Abramowicz, M. A. 2003, PASJ, 55, 69
Nayakshin, S., & Cuadra, J. 2005, A&A, 437, 437
Nayakshin, S., & Cuadra, J. 2007, A&A, 465, 119
Nayakshin, S., Cuadra, J., & Springel, V. 2007, MNRAS, 379, 21
Odaka, H., Aharonian, F., Watanaba, S., et al. 2011, ApJ, 740, 103
Parker, E. N. 1963, Interplanetary Dynamical Processes (New York: Interscience)
Quataert, E. 2002, ApJ, 575, 855
Quataert, E. 2004, ApJ, 613, 322
Quataert, E., & Narayan, R. 1999, ApJ, 516, 399
Revnivtsev, M., Molkov, S., & Sazonov, S. 2006, MNRAS, 373, L11
Rockefeller, G., Fryer, C. L., Melia, F., & Warren, M. S. 2004, ApJ, 604, 662
Ruffert, M., & Melia, F. 1994, A&A, 288, L29
Sazonov, S., Sunyaev, R., & Revnivtsev, M. 2012, MNRAS, 420, 388
Schartmann, M., Krause, M., & Burkert, A. 2011, MNRAS, 415, 741
Schödel, R., Morris, M. R., Muzic, K., et al. 2011, A&A, 532, 83
Spitzer, L. 1962, Physics of Fully Ionized gases (New York: Interscience)
Stone, J., Pringle, J., & Begelman, M. 1999, MNRAS, 310, 1002
Sunyaev, R., Markevitch, M., & Pavlinsky, M. 1993, ApJ, 407, 606
Sutherland, R. S., & Dopita, M. A. 1993, ApJS, 88, 253
Tanaka, T., & Menou, K. 2006, ApJ, 649, 345
Vieser, W., & Hensler, G. 2007a, A&A, 472, 141
Vieser, W., & Hensler, G. 2007b, A&A, 475, 251
Wardle, M., & Yusef-Zadeh, F. 1992, Nature, 357, 308
Xu, Y.-D., Narayan, R., Quataert, E., Yuan, F., & Baganoff, F. K. 2006, ApJ, 640, 319
Yuan, F., Quataert, E., & Narajan, R. 2003, ApJ, 598, 301
Yusef-Zadeh, F., & Wardle, M. 2010, in AIP Conf. Proc. 1248, X-ray Astronomy 2009; Present Status, Multi-wavelength Approach and Future Perspectives, ed. A. Comastri et al. (Melville, NY: AIP), 233